Are Fe–N–C Electrocatalysts an Alternative to Pt-Based Electrocatalysts for the Next Generation of Proton Exchange Membrane Fuel Cells?

Xiong Zhang, Lai Truong-Phuoc, Tristan Asset, Sergey Pronkin, Cuong Pham-Huu

Are Fe-N-Cs An Alternative to Pt-based Electrocatalysts for the Next Generation of Proton Exchange Membrane Fuel Cells?

Xiong Zhang,[a] Lai Truong-Phuoc,[a] Tristan Asset,[a] Sergey Pronkin,[a]* Cuong Pham-Huu,[a]**

[a] *Institute of Chemistry and Processes for Energy, Environment and Health (ICPEES), UMR 7515 CNRS-Université de Strasbourg, 25 rue Becquerel, 67087 Strasbourg Cedex 02, France*

ABSTRACT

Notable progresses have been made for low Pt-based and Fe-N-C electrocatalysts for proton exchange membrane fuel cells (PEMFCs) applications. Particularly, the research and development of cost-effective Fe-N-Cs have witnessed significant improvements in the recent years, due to the need of an alternative candidate to the scare, and expensive, platinum. Numerous studies have been exploring the design and optimization of Fe-N-Cs and generally make simple performance comparison with commercial Pt/C catalysts on the basis of rotating disk electrode (RDE) and/or membrane electrode assembly (MEA), thus arguing that said materials are comparable, or could even surpass, Pt/C electrocatalysts. The resulting question, *i.e.* 'are Fe-N-Cs an alternative to Pt-based electrocatalysts in PEMFCs?' is the centerpiece of this review. Here, the

interconnectedness and differences between Fe-N-Cs and Pt-based materials are discussed from fundamental insights to applications in PEMFCs, covering the oxygen reduction reaction (ORR) mechanism, the nature of active sites and its effect on the intrinsic activity, the rational design of catalyst layer, the electrocatalysts performances in PEMFCs and their durability in operating conditions. This review provides a global picture of the current research state in the field of PEMFCs electrocatalysts, focusing onto the two most important types of cathode materials and aiming to shed light on the potential of Fe-N-Cs as replacement for Pt-based catalysts along with pointing out the research directions toward the next generation of PEMFCs.

KEYWORDS: Fe-N-C electrocatalysts, Pt-based electrocatalysts, oxygen reduction reaction, proton exchange membrane fuel cells, durability, catalytic layer.

Graphical abstract

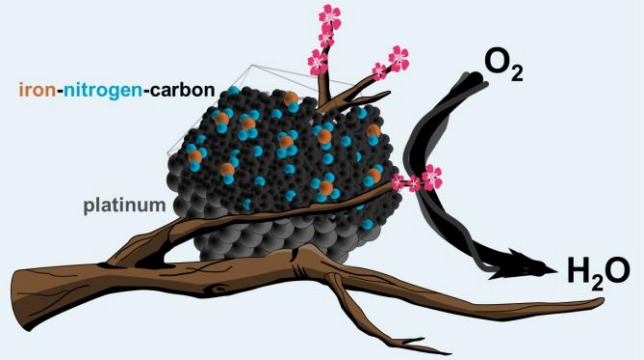

1. Introduction

Addressing the challenges related to the climate change requires the development of green and sustainable energy conversion or storage systems,[1] such as fuel cells. The latter has attracted great research interest throughout the past decades, with one of the key objectives of said research being to meet the energy requirements needed to become an alternative to fossil energy-based systems.[2] Proton exchange membrane fuel cells (PEMFCs) operates through two half-cell reactions, namely the hydrogen oxidation reaction (HOR), and the oxygen reduction reaction (ORR), with electric energy output and pure water as products. The ORR exhibits six or more orders of magnitude slower kinetics than the HOR, hence being the limiting reaction.[3] Nowadays, platinum-based catalysts are generally regarded as the state-of-the-art electrocatalysts for ORR. Loadings as high as 0.4 mg_{Pt}/cm^2 are required to promote the ORR while meeting the requirements for automotive practical application. However, the high cost and scarcity of Pt significantly impede the development of PEMFCs.[4-5] As such, a target of reducing the Pt usage down to 0.1 mg_{Pt}/cm^2 without compromising the PEMFC activity or durability was proposed by United States Department of Energy (DOE) for 2025.[6] Strategies such as alloying Pt with a second, less expensive, metal have been put forward to decrease the Pt loading. This incidentally decreases the cost of the electrocatalyst in the PEMFCs stacks while achieving the enhanced activity owing to the optimized binding energy of the ORR intermediates.[7-8] To date, the DOE 2025 target has been fulfilled (*i.e.* activity of 1.08 $A/mg_{Pt}@0.9V_{IR\text{-}free}$ with 0.033 mg_{Pt}/cm^2 and 36 % losses in mass activity after 30k cycles *vs.* DOE target being an activity of 0.44 $A/mg_{Pt}@0.9V_{IR\text{-}free}$ with

0.1 mg_{Pt}/cm^2 and a durability of < 40 % losses in mass activity after 30k cycles [9]), but long term, large-scale deployment of PEMFCs in the field of automotive production might require the use of elements that are far less scare than Pt. As such, earth-abundant platinum-group metal free (PGM-free) based electrocatalysts and more specifically, metal-nitrogen-carbon (M-N-C) electrocatalysts have been of growing interest, due to their low cost, CO-tolerance and high intrinsic activity toward the ORR.[10-12]

Cobalt phthalocyanine has been proposed in 1964 by Jasinski as an active phase for the ORR.[13] Following this pioneering work, M-N-C electrocatalysts prepared by high temperature pyrolysis of metal-macrocycle complexes adsorbed on carbon substrate were investigated and showed promising ORR activity.[14-15] In 1989, it was reported by Yeager *et al.* that M-N-C electrocatalysts could be synthesized through pyrolysis of separated metal, carbon and nitrogen sources which enabled better flexibility and control of the electrocatalysts physico-chemical properties.[16] To date, tremendous progresses have been achieved for the preparation of Fe-N-C electrocatalysts (iron being considered as the best 3d-transition metal for M-N-C applied to the ORR) leading to high performances in fuel cells. Very recently, the catalytic activity (0.0442 A/cm^2@0.9 $V_{IR\text{-}free}$) or durability (30 mV losses at 0.8 A/cm^2 after 30k cycles) of Fe-N-C-containing PEMFCs reached the DOE targets (0.044 A/cm^2@0.9 $V_{IR\text{-}free}$, ≤ 30 mV losses at 0.8 A/cm^2 after 30k cycles) for 2025 [17], although not simultaneously. In the light of those exciting achievements for both Fe-N-Cs and Pt-based catalysts, getting a comparison statement between both electrocatalysts' families is of extreme interest. Such is the aim of this review that will cover, on both Pt-based electrocatalysts and Fe-

N-Cs (1) the ORR mechanism; (2) the nature of active sites and their plurality; (3) the intrinsic activity regulation; (4) the structural engineering of cathode catalyst layer in PEMFCs; (5) the degradation mechanisms. Finally, outlooks and challenges are addressed to answer the question brought forth in this review, *i.e.* the alternatives to Pt-based electrocatalysts provided by Fe-N-Cs.

2. The ORR mechanism of Pt/C *vs.* Fe-N-C

One must first clarify fundamental mechanistic insights for the ORR mechanism on both Fe-N-Cs and Pt based electrocatalysts to be able to establish a meaningful comparison. The ORR proceeds by either four-electron ($4e^-$) pathway with H_2O (acidic media) and OH^- (alkaline media) as primary reduction products or two-electron ($2e^-$) pathway with H_2O_2 (in acid) and HO_2^- (in alkaline) as main products.[18-19] The detailed mechanism in acidic media can be divided into three pathways as shown in **Figure 1A**. Typically, the oxygen molecule is first adsorbed and activated on the surface of catalyst to form O_2* (herein the * is denoted as active site of catalyst), followed by O-O bond cleavage in three different manners, (1) dissociative pathway: the O-O bond in O_2* is cleaved directly into two O* intermediates, which are then successively reduced to OH* and H_2O* and eventually end up with desorption of H_2O*, (2) associative-dissociative pathway: OOH* is first generated from O_2*, then the O-O bond in OOH* is cleaved into O* and OH*, followed by their successive reductions to form H_2O, (3) the associative pathway: the O_2* is sequentially reduced to OOH* and HOOH*, then 2 OH* can be generated and finally reduced to H_2O*. For most catalysts (*e.g.* Pt (111) and four

electron-dominated Fe-N-Cs), the associative-dissociative pathway is considered as dominant.[20-21]

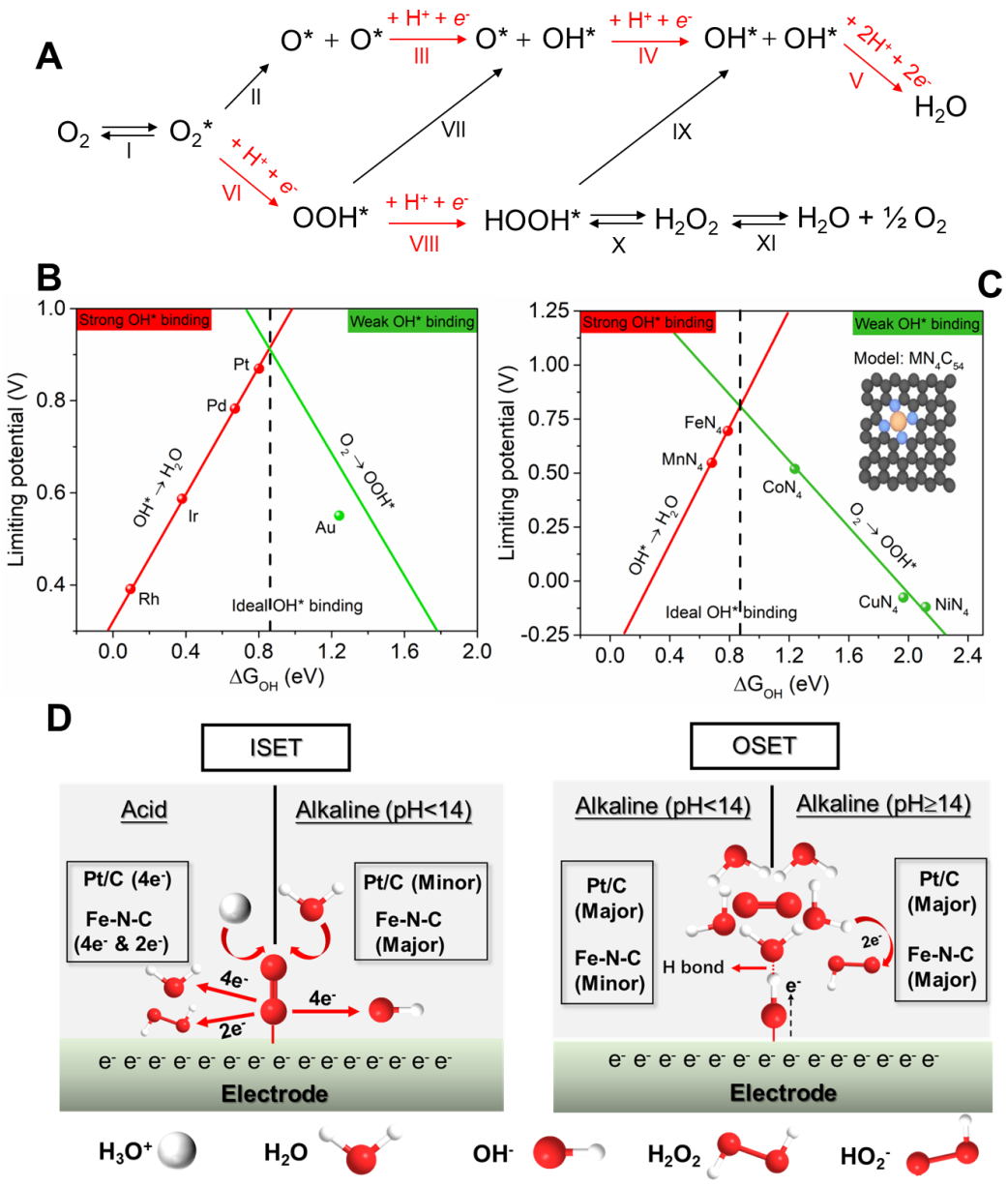

Figure 1. (A) The generalized reaction pathway toward ORR; the red lines correspond to steps involving a proton and an electron (*i.e.* either proton coupled electron transfer or sequential electron transfer/proton transfer); (B) the limiting potential plot for various metal catalysts as a function of OH* Gibbs free energy (ΔG_{OH}), adapted from Ref. 21; (C) the limiting potential plot for various M-N-Cs (M = Fe, Co, Mn, Cu, Ni) catalysts as a function of ΔG_{OH}, adapted

from Ref. 22; (D) The ISET (inner sphere electron transfer) and OSET (outer sphere electron transfer) mechanisms comparison between Pt/C and Fe-N-C. For the ISET, in the case of acid media, the unstable binding of generated H_2O_2 intermediate onto Fe(II)-N_4 leads to partial desorption of H_2O_2 and thus, an incomplete $2e^-$ reduction. In sharp contrast, under mild (pH < 14) alkaline medium, the stable adducts HO_2^- -Fe(II)-N_4 lead to a complete reduction of the HO_2^- to OH^-, whereas an OEST begins to dominate in ORR for Pt/C. Notably, OSET is observed for both Pt/C and Fe-N-C at pH ≥ 14 due to full OH^- coverage on the electrode surface.

The association-dissociative pathway typically involves three oxygen intermediates, *i.e.* OOH*, O*, OH* (**Figure 1A**) and the theoretical electrocatalytic activity is strongly dependent of their binding free energies. Nørskov's group [21, 23-24] proposed the following scaling relations between each of the aforementioned intermediates, *i.e.* $\Delta G_{OH*} = 1/2\ \Delta G_{O*}$ and $\Delta G_{OH*} = \Delta G_{OOH*} - 3.2$ eV, thus implying that the catalyst surface reactivity can be quantified as the function of one binding energy, *e.g.* OH*. According to the Sabatier principle, the ideal ORR electrocatalyst should bind its intermediates species neither too strong nor too weak.[25] This results in the existence of volcano-plot like correlation between the activity and the binding energy of the intermediates (**Figure 1B** and **1C**). Among all investigated elements, Pt exhibits the closest-to-optimum OH* binding energy, being only 0.1 – 0.2 eV too strong. This can be further improved through modulation of its electronic structure (*e.g.* downshifting the 5d-band center of the Pt surface) to decrease its affinity toward OH* species. A similar volcano plot is also established for several 3d-transition metal-N-C catalysts, as shown in **Figure 1C**. Fe-N-C appears as the most active M-N-C, owing to its FeN_4 active site and binds OH* slightly too strongly as well, thus implying that modifying its 3d-band structure might

also results in activity enhancement. Interestingly, the apex potential for extended metallic surfaces is *ca.* 100 mV higher than for M-N-Cs (**Figure 1B** and **1C**), hinting toward an intrinsically inferior activity for Fe-N-Cs *vs.* Pt-based catalysts.

The ORR selectivity (H_2O_2 *vs*. H_2O) mainly depends on the dissociation energy barrier of absorbed O_2 molecule on the surface of the active site. The O_2 dissociation energy barrier on pure carbon materials surface is relatively high due to the weak oxygen adsorption, thus favoring H_2O_2 generation.[21, 26] On the contrary, the O_2 dissociation energy barrier (dominated by associative-dissociative pathway as previously mentioned) on metal surfaces or metal-doped nitrogen-carbon surface is much lower, thus greatly favoring the $4e^-$ pathway for both Pt and Fe-N-C catalysts.[27-28] The first charge transfer (Step VI in **Figure 1A**) is considered as the determining step (RDS) for both Pt and Fe-N-C electrocatalysts.[29-31] Tse *et a*l.[32] evidenced the RDS of Pt does not involve a proton transfer step, *i.e.* $Pt + O_2 + e^- \rightarrow Pt\text{-}OO^{*-}$, which was later confirmed by George *et al.* and Talarposhti *et al.* in acidic media, owing a high density of Pt nanoparticles onto the carbon surface.[33-34] In opposition to Pt catalyst, the RDS of Fe-N-C involves a proton-coupled electron transfer (PCET), *i.e.* $N_x\text{-}Fe + O_2 + H^+ + e^- \rightarrow N_x\text{-}Fe\text{-}OOH^*$.[32] This would suggest that in acidic media, the ORR performance of Fe-N-C electrocatalyst is intrinsically inferior to that of Pt catalyst due to the increased complexity of the PCET on the Fe-N-C. Chen *et al*.[30] proposed that the PCET was arising from the $2e^-$, H_2O_2 generating pathway, thus implying that the $4e^-$ transfer was proton-independent. Such independence would underline that (i) minimizing the $2e^-$ pathway selectivity on Fe-N-C is critical and (ii) owing that the proton independency is upheld, the Fe-N-Cs would

not be limited by the slow PCET and therefore could potentially complete with Pt-based electrocatalysts.

The ORR process is complicated not only because of multiple electron and proton transfer steps, but also due to the pH dependence of its mechanism. Here, the ORR mechanism as a function of pH is elucidated for both Pt and Fe-N-C. To understand the mechanism, one must first understand the chemical state of the double-layer, which has been discussed in details in the pivotal works of Ramaswamy and Mukerjee:[35-36] (i) in acidic media and operating ORR conditions, the inner-Helmholtz plane (IHP) consists of chemisorbed O_2, OH* and H_2O dipoles, whereas the outer-Helmholtz plane (OHP) consists of solvated O_2, electrolyte anions and H_3O^+; (ii) in alkaline media and operating ORR conditions, the double-layer chemistry is similar, the notable differences being the alkali metal ions replacing the protons from the acidic environment and the fact that the OH* now arises from direct OH^- adsorption rather than H_2O activation at high potentials. This directly impacts both the Pt and Fe-N-C reactivity: (i) for Pt, in acidic media, the ORR occurs through reduction of the adsorbed O_2 in the IHP, in concert with proton transfers from the OHP to the IHP, leading to a $4e^-$ reduction without desorption of the intermediate (**Figure 1D**); (ii) in alkaline environment, two mechanisms are observed, owing to the partial formation of an oxide layer onto the Pt surface: an inner sphere electron transfer (ISET) on oxide-free Pt-sites where O_2 can chemisorb, which leads to a $4e^-$ transfer, similarly to (i); a non-surface specific outer sphere electron transfer (OSET) on the Pt-oxide, where the solvated O_2 forms an hydrogen bond with the OH* that ultimately leads to a $2e^-$ pathway and HO_2^- generation (**Figure 1D**). Logically,

the OSET contribution increases with the OH* coverage and, thus, dominates in strong alkaline environment on Pt (pH ≥ 14), as illustrated in **Figure 1D**. The domination of the $2e^-$ pathway at pH ≥ 14 also occurs on Fe-N-C. On the latter, (i) little to no contribution of the $2e^-$ pathway is observed in mild alkaline solution (at pH < 14), indicating that O_2 adsorption on the Fe-N_x center is favored over OH* formation, leading to the formation of HO_2^-. Said reduction is (ii) not favorable in acidic environment, owing to the weak H_2O_2 binding on the active sites, thus leading to a mix of H_2O_2 and H_2O being generated on Fe-N-C (see **Figure 1D**).[36-37] In summary, in alkaline environment, the Pt surface gradually becomes (with the pH increases) non-specific and dominated by $2e^-$ pathway, whereas Fe-N-C electrocatalysts mainly follow a $4e^-$ pathway. In acidic environment, the ORR on Pt/C occurs through the $4e^-$ pathway, whereas lower selectivity and H_2O_2 generation is observed on Fe-N-C. The pH variation induced by the alkaline *vs.* acid environment also indirectly impacts the Fe-N-Cs by modifying the chemistry of the nitrogen [38-39] neighboring the Fe-N_x actives sites (*e.g.* stronger withdrawing electron effect from N-H respect to N^- induced by protonation of pyridinic N from alkaline to acidic media, thus affecting the 3d-band density of iron atoms).

In this section, we underlined that (i) both Fe-N-C (through its Fe-N_4 moiety) and Pt are respectively the best M-N-C and best element for the ORR, although they bind the oxygen intermediates slightly too strongly; (ii) both electrocatalysts families follow a dissociative-associative pathway (or associative for the Fe-N-Cs with low selectivity). The low selectivity of the Fe-N-Cs in acidic media, along with a PCET being the rate determining step on the $2e^-$ pathway, are here identified as two of the key limiting

aspects of the Fe-N-Cs when being compared to Pt-based electrocatalysts. To overcome them, one direction would be to finely tune the electronic properties of the active sites, along with the chemical surface properties of the Fe-N-Cs, to slightly decrease the OH* binding energy and to increase the ORR selectivity toward a $4e^-$ pathway. However, before proposing structural modifications, one must understand the nature, and plurality, of the Fe-N-Cs active sites, which diversity is equal to the one of Pt-based electrocatalysts.

3. The nature of active sites for Pt-based electrocatalysts and Fe-N-Cs

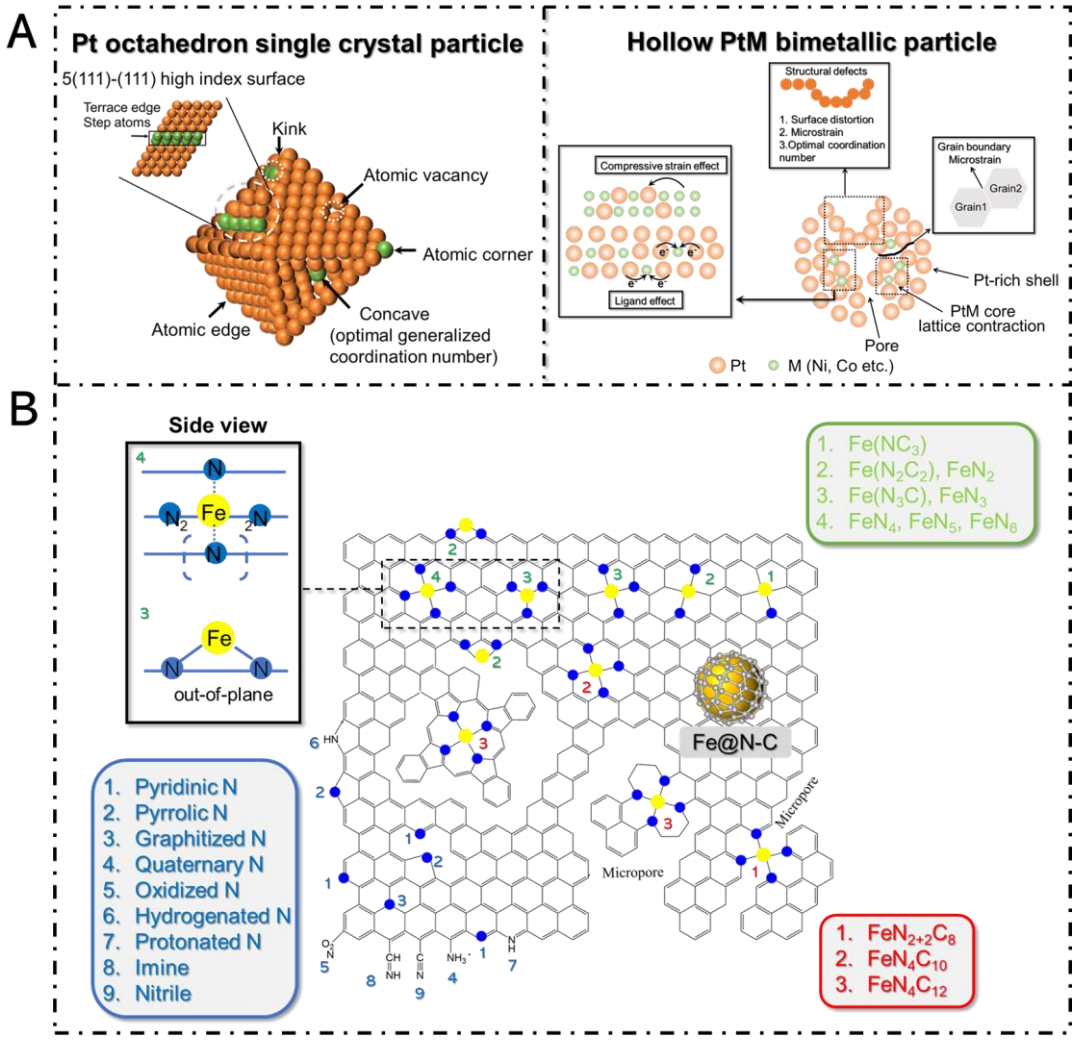

Figure 2. The nature of active sites (A) of Pt-based electrocatalysts (using a Pt octahedron single crystal (111) particles (left) and hollow PtM bimetallic particle (right) as example); and (B) of the various FeN_x-containing, N-containing and metallic nanoparticles discussed in the literatures on Fe-N-C electrocatalysts.

Each accessible platinum atom contributes, to a certain extent, to the ORR. For Pt-based nanoparticles, the activity strongly depends on (i) the Pt atom coordination and (ii) its average distance with its closest neighbors. Both strongly impact the Pt electronic structure and, thus, the OH* binding strength. This was the first observed on

monocrystalline surfaces, by investigating different crystalline orientations and showing that Pt (110) > Pt (111) > Pt (100) in terms of activity.[40] This order changes when switching from Pt to Pt_3Ni, *i.e.* Pt_3Ni (111) > Pt_3Ni (110) > Pt_3Ni (100), hence explaining the interest for Pt_xNi structures with high (111) facets density, *e.g.* octahedra [41]. Interestingly, the activity of the basal planes is modified in presence of steps, atomic vacancy, *etc*.[42-47] (see **Figure 2A** left). Specifically, it appears that the high-coordinated 'bottom-of-the-step' site is key for the ORR on Pt extended surfaces. Further investigation by Calle-Vallejo and Tymoczko *et al.*[48] evidenced that an optimal active site should exhibit a generalized coordination number (*i.e.* a coordination number considering the first and second row of neighbors) of 8.3, whereas Le Bacq *et al.*[49] underlined the key role played by the interatomic distance of a given active site onto its activity. Those aspects play a fundamental role in the design of Pt-based ORR electrocatalysts: (i) the optimized mass activity for Pt nanoparticles is observed in the size of 2-3 nm.[50-51] Further downsize of the Pt nanoparticles results in inferior intrinsic specific activity due to dominating low-coordinated steps and kinks leading to too strong oxygen binding.[50] Incidentally, this explains why single Pt atoms or Pt nanoclusters (albeit promising in terms of Pt utilization [52-53]) present a low intrinsic activity for the ORR, *i.e.* because of their extremely low coordination and the resulting too strong binding of the intermediates species;[48] (ii) as observed in **Figure 1B**, Pt (111) shows a slightly too strong adsorption strength of the oxygen intermediates, which can be optimized by following three approaches, namely (a) designing PtM (M = 3d-transition metals [40, 54] or rare-earth elements [55-56]) without modifying the coordination or nanoparticle size, leading

to an activity improvement through strain [57-59] and ligand [60] effects (for the 3d-transition metal) along with more complex structural modifications (*e.g.* Kagome layer for the rare-earth elements,[55] grain boundary,[61] structural defects,[61-62] surface distortion [63] *etc.*) (see **Figure 2A** right). Indeed, those effects result in the alteration of the Pt 5d-band electronic structure and, as such, a near-optimal oxygen-based adsorbates binding energy (b) optimizing the structure through the design of shape-controlled nanostructures, aiming to expose preferential facets of Pt to maximize the catalytic activity.[64-65] (*e.g.* Pt_3Ni octahedra dominated by (111) facets, see **Figure 2A** left) (c) implementing structural defects into the Pt-based nanostructures, aiming to design active sites with an optimal generalized coordination number and optimal atomic distance with the nearest neighbors and, therefore, an optimal binding energy for the ORR intermediates.[48, 61] Those different approaches led to a wide range of highly performing, innovative Pt-based electrocatalysts, that are discussed in further extent in Ref. [47, 61, 66].

Similarly to Pt-based electrocatalysts, the Fe-N-C electrocatalysts derived from separated iron, carbon/nitrogen precursors present a wide diversity of active sites. However, where the Pt-based electrocatalysts active sites diversity arises from the distance, and coordination, with other platinum atoms, the Fe-N-Cs diversity arises from the presence or absence of Fe, along with the coordination with nitrogen. Specifically, as shown in **Figure 2B**, three type of active sites are observed: (1) atomically dispersed iron moiety (FeN_xC_y), (2) N-doped carbon moiety (C-N), (3) iron-based nanoparticles. The precise identification of FeN_xC_y coordination shells (x, y values) remains challenging and is conventionally extrapolated from Mössbauer spectroscopy [67] and X-ray

adsorption spectroscopy, more specifically, extended X-ray adsorption fine structure (EXAFS).[68] The possible Fe-N_x coordination number in the first shell is proposed to be x = 1 - 4, based on experimental and theoretical calculation findings [69-76] (**Figure 2B**). Notably, on the basis of EXAFS and Mössbauer findings, recent works have been discussing higher coordination numbers, including the presence of a nitrogen atom below the plane, thus leading to a N-FeN_4 [77-80] or N-FeN_4-N [81-82] structure (left inset in **Figure 2B**). The chemistry and relative abundancy of the Fe-containing moieties are usually controlled by two parameters, *i.e.* (i) the pyrolysis temperature [69, 82] and (ii) their position in the carbon structure, *i.e.* FeN_2 is commonly observed on the edge of the carbon crystallite [83] while FeN_3 and FeN_xC_{4-x} (where C is located at first coordination shell with $x \leq 4$) moieties are observed in-plane (Figure 2B).[74, 83] The first and second coordination shell of the moiety most often considered as best for the ORR, the FeN_4, is widely debated,[84] and often established from a combination of Mössbauer and EXAFS findings combined with modelling. Hence, it is essential to look to this discussion with a critical eye, *i.e.* (i) the fitting of the Mössbauer/EXAFS data can often correspond to several geometries and (ii) the pyrolytic methods undergone to synthesize the Fe-N-Cs lead to the presence of a wide variety of coordination/chemistry, *i.e.* that there is not one type of active site in a given electrocatalyst. Unfortunately, obtaining a direct proof of the existence of a given coordination (*e.g.* by high resolution electron microscopy combined by elemental mapping) is extremely challenging on Fe-N-Cs synthesized by pyrolytic methods, leaving the exact nature of the active sites as hypotheses, albeit strongly backed with indirect evidences. Furthermore, inadequate characterization

procedure can also affect the obtained data and, thus, the interpretation. For example, for Mössbauer spectroscopy, low temperature is required for a precise identification of the different moieties, as α-Fe_2O_3 nanoparticles share similar Mössbauer parameters to FeN_4C_{12} sites at room temperature.[85-86]

On the basis of Mössbauer spectrum results, Kramm *et al.*[79-80] originally proposed that the Fe-containing moieties consisted of low spin (here referred as D1, and considered as a Fe(II)-N_4 moiety), intermediate spin (D2, Fe(II)-N_{2+2}, Fe situated between two carbon crystallites) and high spin (D3, N-Fe(II)-N_{2+2}, Fe situated between two carbon crystallites with N-graphitic in the plane underneath the Fe atom or FeN_{4+1} with adjacent protonated nitrogen). Only D1 and D3 sites were deemed to exhibit high ORR activity while D2 was considered as inactive due to the Fe fully occupied 3d orbital failing to bind O_2 in a non-bent conformation. Although the D3 sites are proposed to be most active site for ORR,[79-80] they are preferentially hosted in micropores,[87] which compromises their performance in PEMFC operating conditions due to their inaccessibility to ionomer,[88] flooding and demetallation [89-90]. In recent studies, Mukerjee's group [91-93] provided further insights on the D1 moiety and its variations as a function of potential, ascribing it to high spin 'in-plane' OH-Fe(III)-N_4 sites (axially coordinated to oxygen from water activation) at high potential and 'out-of-the-plane' Fe(II)-N_4 sites at low potential, the latter being considered as the active site [94] while the site-blocking effect resulted from water activation was viewed as detrimental. [85, 94-95] In this end, intrinsic activity could be significantly improved by increasing the Fe(III)/Fe(II) redox transition potential.[94, 96] The local carbon structure in the second shell surrounding the

FeN_4 moiety also varies on distinct FeN_4C_y sites: 'y' values are found to be eight (*i.e.* $FeN_{2+2}C_8$, micropore sites, bridging two carbon crystallite) [97-99], ten (*i.e.* FeN_4C_{10}, bound to pyridinic N),[85] or twelve (*i.e.* FeN_4C_{12}, bound to pyrrolic N) [68, 85, 100]. The FeN_4C_{12} moieties, surface accessible, correspond to the D1 doublet [100-101]. The moiety location is also of critical importance when addressing the material stability, *e.g.* FeN_2, $FeN_{2+2}C_y$ moieties are edge sites while FeN_4C_y, FeN_3 and FeN_xC_{4-x} moieties are more likely 'plane-exposed' sites (*i.e.* situated in the carbon basal plane facing the mesopore, **Figure 2B**).[83, 102-103] Hence a mesoporous carbon favors FeN_{4+1}, FeN_4C_y, FeN_3, FeN_xC_{4-x} as main active sites, whereas more 'edge-exposed' (*e.g.* armchair, zig-zag edge of carbon basal plane and micropores) lead to FeN_2 and $FeN_{2+2}C_y$ as main active sites. Noteworthy, the carbon edges are preferentially corroded, thus suggesting that, from a durability standpoint, the development of 'plane-exposed' sites should be favored.

Assessing the reactivity of Fe-based nanoparticles (metallic Fe, iron oxides, carbides and nitrides) observed in highly loaded Fe-N-Cs remains challenging, due to the simultaneous presence of FeN_xC_y sites. Extensive studies have revealed that they act as the main ORR active site in alkaline medium.[104-111] Specifically, a synergetic effect between Fe-nanoparticles and FeN_xC_y moieties has been widely proposed.[112-120] For instance, in alkaline media, Wei's group [121] proposed that Fe/Fe_3C nanoparticles could dramatically improve the activity of the adjacent $Fe\text{-}N_x$ by modifying the electronic structure of the latter, which favored the O_2 adsorption. In acidic media, the Fe-based nanoparticles (Fe/Fe_3C) encapsulated into thin graphitic N-doped carbon layer (Fe@N-C, see **Figure 2B**) usually present an excellent ORR activity and durability.[122-129]

However, the encapsulated Fe-based nanoparticles are not involved in the ORR process, but exert a positive electronic effect on the outer surface of graphitic carbon layer that favors the stabilization of the H_2O_2 intermediates and enables full $4e^-$ ORR.[124-125, 128] More importantly, they are protected from direct contact with the electrolyte and H_2O_2 intermediates, thus exhibiting high stability.[124, 128] Indeed, Choi *et al.*[130] recently confirmed that these carbon-encapsulated Fe nanoparticles (Fe@N-C) electrocatalysts presented a high ORR activity leading to $4e^-$ reduction, dominated by the indirect four electron oxygen reduction (S*, see **Figure 3**, $O_2 \rightarrow H_2O_2$ and $H_2O_2 \rightarrow H_2O$) associative pathway. However, 'electrolyte-exposed' iron-based nanoparticles are ORR inactive in acidic environment, as revealed by the independence of the ORR activity on their presence.[130-132] As such, the latter should be avoided in acidic environment as it also contributes, through its corrosion during operation, to the poisoning of membrane and the formation of strong oxidative radical $HO^{\bullet}$ by Fenton reaction.[131-132] Mitigation methods, such as the use of sulfur-based precursors, have been recently introduced to prevent their excessive formation.[133-135] Overall, the contribution to the catalytic activity of the iron-based nanoparticles in acidic environment strongly depends on the thickness of the N-doped carbon shell surrounding them, which itself depends of the synthesis procedure (*e.g.* pyrolysis temperature and type of carbon, nitrogen precursors).[136-137] Altogether, the improved ORR performance can be achieved through (1) increasing the sites density of atomic, D1, FeN_xC_y sites or rational design of Fe@N-C site with proper coated N-doped carbon layer; (2) removing the naked Fe-based nanoparticles to prevent the poisoning of membrane or the formation of high corrosive reaction radical species

(ROS) induced by Fenton reaction due to the dissolution of Fe nanoparticles during ageing.[131-132]

Nitrogen atoms are also incorporated into carbon matrix during pyrolysis as iron-free, nitrogen-containing functionalities. Such nitrogen species in carbon matrices have been assigned by X-ray photoelectron spectroscopy and density functional theory (DFT) calculations, including imine or nitrile groups (≤ 398.0 eV),[138] pyridinic N (398.3 – 398.8 eV),[139] amine group (399.5 – 399.8 eV),[138-139] pyrrolic N or hydrogenated N (400.6 – 400.9 eV),[139-140] and a mixture of quaternary N, graphitic N and protonated pyridinic N (401.5 – 403.0 eV),[138, 141-142]. The nitrogen-based moieties are highly sensitive to their chemical environment, with different binding energies observed for chemically identical moieties (*e.g.* pyridinic) if they are found in the basal plane or on the carbon edge.[139] The N-containing functionalities only catalyze part of the ORR: in acidic media, whereas FeN_xC_y and Fe@N-C sites are S or S* with direct four electron reduction or single site series 2×2 e^- electron reduction processes (see **Figure 3**); the pyrrolic N, protonated or hydrogenated N, quaternary N (N^+) and graphitic N are S1 sites ($O_2 \rightarrow H_2O_2$, **Figure 3**) and pyridinic N is a S2 site ($H_2O_2 \rightarrow H_2O$, **Figure 3**).[130, 138-139, 142-143] The exact nature of the pyridinic N site is still controversial, with Guo *et al.* [144] suggesting that the latter is responsible for a Lewis-basic behavior of the neighboring carbon atoms, but Kondo *et al.*[145] arguing that the lone pair on the pyridinic nitrogen implies a negatively charged nitrogen and thus that the surrounding carbon atoms should be positively charged, rendering them inadequate as a Lewis base. This should be also considered in the prism of the pH variations, as the phenomena changes

in acidic environment, with the protonation of the pyridinic N (pK_a = 6.5) [37-39, 146-147] that modify its charge delocalization and thus, in theory, the Lewis basicity of the adjacent carbon atoms. Notably, N-containing moieties exhibit nearly no activity or far lower ORR activity in acidic environment, with respect to FeN_xC_y moieties. [83, 130, 146] Furthermore, they act as defects in the carbon structure and, therefore, starting points for degradations during operation in acidic environment, although this defectivity can be positively used to tune the electronic structure of the iron, as explored in the following section.

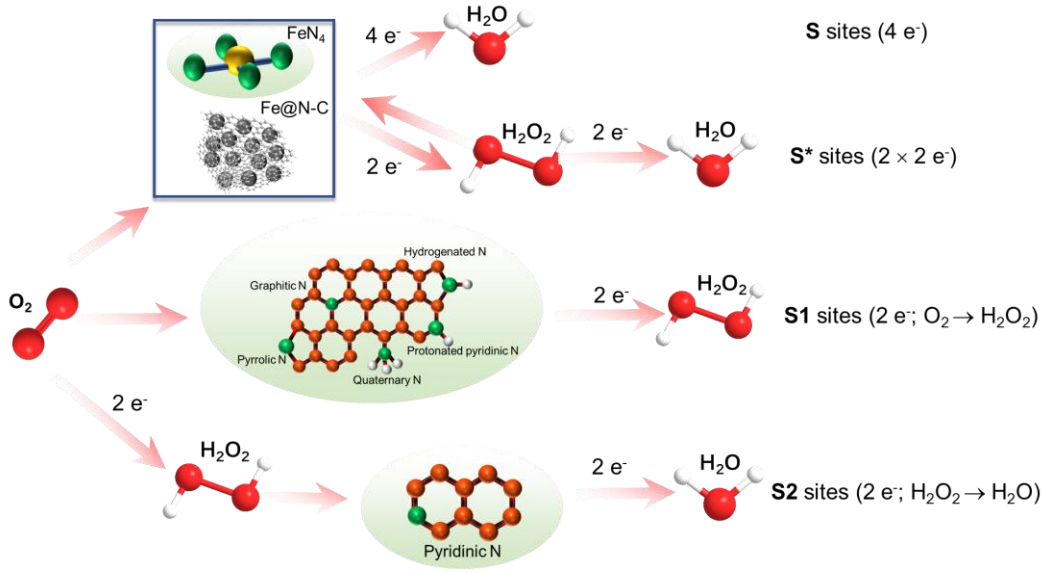

Figure 3. The ORR reaction pathway on the distinct active sites in the Fe-N-Cs electrocatalysts.

The quantification of the active sites in both Pt-based and Fe-N-C electrocatalysts is also of critical importance. CO as a molecular probe has been widely applied to quantify the active site for Pt-based catalysts by means of chemisorption or CO electrochemical stripping,[148-149] whilst no or extremely weak adsorption of CO at room temperature

or under potential was observed on Fe-N-C electrocatalysts.[150-151] A variety of probe molecules (*e.g.* CN^-,[152-154] H_2S,[155] SCN^-,[156] SO_2,[156] NO,[67] *etc.*) thus has been extensively employed as poisoning agents to quantify the active sites in Fe-N-Cs. Sahraie *et al.*[157] have successfully quantified the bulk and surface-based density of Fe-N_x sites using low-temperature CO pulse chemisorption, and the positive correlation between CO uptake and kinetic current density in acidic medium evidenced that CO molecule was predominantly adsorbed on surface sites. Kucernak *et al.* [158] developed a protocol that allowed the quantification of the Fe-N_x sites by means of nitrite adsorption followed by reductive stripping operated at pH = 5.2. Such strategy represents the most advanced methodology for quantification of Fe-N_x active sites to date.[159] It is worth noting that the interaction between nitrite ion and iron center can be significantly impacted by the FeN_x sites surroundings (*e.g.* the presence of basic groups neighboring the FeN_x sites exert an electron-donating effect on Fe thus weakening the chemisorption of the nitrite anion on the Fe center), which limits the its application in some certain catalysts, as revealed by Kumar and Asset *et al.*[160] Furthermore, these methods only apply to FeN_x moieties, *i.e.* Fe-based nanoparticles and Fe-free moieties cannot be assessed by such means. Interestingly, both Fe-N-Cs and Pt-based electrocatalyst show some similarities in terms of active sites: (i) both present a wide variety of potential active sites for the ORR, for which structure-activity relationships will be established in the next section and (ii) structural defects in the electrocatalysts structure are interesting, as they either lead to the formation of ideally coordinated active sites, with optimal nearest-neighbor distance (for Pt-based), or to a higher density of iron, nitrogen-

based moieties that are crucial for the oxygen reduction activity. Furthermore, the atomically dispersed nature of the iron site, *vs.* the mandatory minimal size of the Pt nanoparticles to access a relevant intrinsic activity, imply a far higher utilization of the former, which, owing an optimal loading and dispersion, could lead to extremely high activity, comparable to platinum electrocatalysts.

4. The regulation of ORR intrinsic activity on Fe-N-Cs and Pt-based electrocatalysts

4.1. π-electron delocalization of carbon basal plane on Fe-N-Cs

According to the previous analysis, the Fe(II)-N_4 site is deemed to be the most important Fe-N-C's site for the ORR. It is located on the strong adsorption side of the volcano plot (**Figure 1C**). When addressing this sole moiety, it appears that its catalytic activity is governed by d-electron density of iron, as the alteration of d-band center greatly affects the type, and strength, of the bonding between the Fe center (d_{z2} orbital) and molecular O_2 or oxygenated intermediate (π* anti-bonding orbital).[161-163] The d-electron density of the iron center can be regulated by the surrounding π-conjugated ligand or carbon basal plane with various donating- or withdrawing-electron properties.[164-165] Ramaswamy *et al.*[165] observed that, during the pyrolysis of iron macrocyclic complex, the Fe-N_4 active site switched from a π-electron rich macrocyclic ligand environment to a relatively π-electron deficient graphitic carbon environment, which resulted in a decreased electron density at the Fe center and a downshifted d-band center of Fe, thus optimizing the adsorption strength of ORR intermediates and leading to an

higher turnover number. Further optimization of OH* binding energy on FeN_4 moieties can be performed through modification of the carbon basal plane: increasing the density of structural defects (edge, hole, heteroatom-doping) or disorder degree (lower graphitization degree) disrupt the π-electron delocalization, which further increases the electron withdrawing nature of the carbon plane, thus downshifting the d-band center and enhancing the ORR (see **Figure 4A**). On the contrary, a highly graphitized carbon surface with fewer defects results in an increased electron donating property and a stronger OH* binding, therefore compromising the ORR activity (**Figure 4A**). It is worth noting that, although increasing the structural defects density can potentially optimize the ORR activity, highly defective carbon planes ('overshooting') will not only result in too weak OH* binding energy (shift to the right side of volcanic plot, **Figure 4A**) but also reduce their durability due to large number of preferential corrosion sites.[17, 83] Taken together, a trade-off between graphitization degree and structural defects should be carefully considered for optimization of both intrinsic activity and durability.

4.2. Ligand effect surrounding FeN_4 site.

In addition to the effect of π-electron delocalization of carbon basal plane on d-electron density of Fe center, the so-called ligand effect also plays an important role in tuning the ORR activity.[166] A variety of element dopants with distinct electronegativity have been investigated, with sulfur-doping being the most commonly studied.[167-173] Generally, the S-doping does not affect the coordination of Fe center: the sulfur atom is either adjacent or away from the nitrogen atoms in the FeN_4 site.[174-175] Two forms of S dopants with electron-withdrawing oxidized S ($C\text{-}SO_x$) [176] and electron-donating

thiophene-like S (C-S-C) [175-178] are proposed to tune the electron structure of the FeN_4 moiety. Specifically, the introduction of oxidized sulfur (-C-SO_x) [176] on the neighboring FeN_4 sites significantly decreases the d-band center of Fe by an electron-withdrawing effect, which shifts OH* binding energy toward the apex direction of the volcano plot (**Figure 4A**). On the contrary, the thiophene-like C-S-C increases the electron density of the Fe center due to a strong electron-donating effect thus brings the electrocatalyst toward the stronger adsorption energy side (**Figure 4A**). Besides S-doping, other elements such as B,[179-180], P,[181-183] and O [184] with different withdrawing/donating groups are also documented. Independently of the dopant nature, it is important to note that (1) the effect on the d-band center strongly depends on the distance between the dopant and the FeN_4 moiety;[178] (2) as aforementioned for the structural defects, the content of dopants should be carefully controlled so as to obtain optimal binding energy on Fe center (*e.g.* excessive amount of C-SO_x or electron-withdrawing groups resulting in too weak OH* binding on FeN_4 sites-right side of volcano plot, **Figure 4A**).

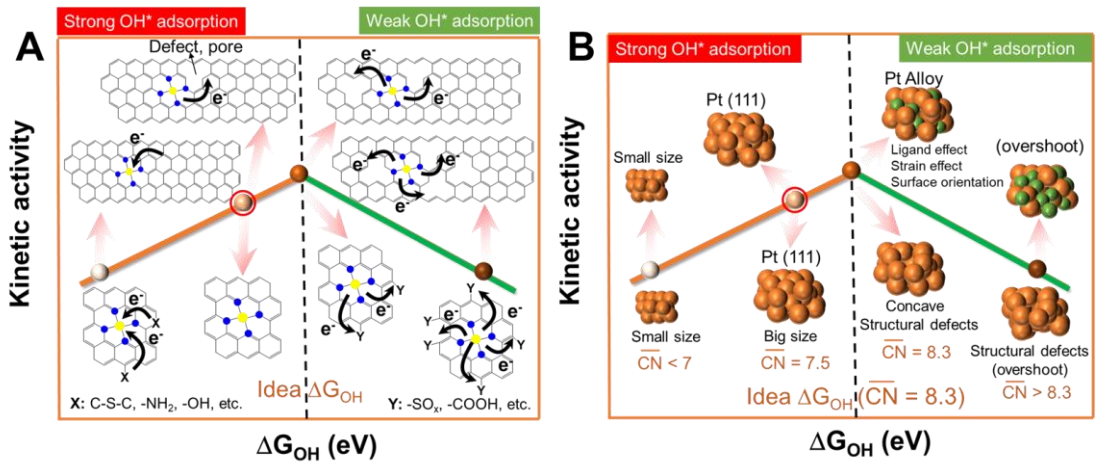

Figure 4. Schematic illustration of activity regulation by the modification of the electronic structure of the active site on Fe-N-C electrocatalysts (A), and Pt-based electrocatalysts (B)

aiming to improve the ORR intrinsic activity.

4.3 The regulation of intrinsic activity of Pt-based catalysts

Tuning the surroundings of a given active site echoes with the recent efforts undergone to design innovative Pt-based electrocatalysts, as touched upon in Section 3, and that Sabatier-driven, volcano-shaped activity is easily applied to this family of electrocatalysts as well. Indeed, considering Pt (111) as the 'Fe(II)-N_4 like' site, binding OH* 0.1 - 0.2 eV too strongly, it appears that, as illustrated on **Figure 4B**: (1) the addition of 3d-transition metals and/or the use of clearly defined crystalline orientations (*e.g.* Pt_3Ni(111), octahedra, nanoframes) lead to a downshifting of the Pt 5d orbital and the resulting weakening of the OH* adsorption strength, thus greatly increasing the ORR activity.[40-41, 185] But such modification also impacts the nanostructure durability, as well-organized facets and 3d transition metals both exhibit low stability in highly acidic environment;[63, 186] (2) properly decreasing the Pt nanoparticles size enables more exposure of active sites, but excessive downsizing exposes a large density of edges sites with decreased coordination number (**Figure 4B**). This negatively impacts the ORR activity due to too strong OH* adsorption as well as decreasing the nanoparticles durability due to the easier aggregation of small particles induced by large surface energy; (3) the addition of localized structural defects (*e.g.* platinum adatoms, concavities) modifies the local environment of a given platinum atom and, through the changes in its microstrain and local coordination, thus its OH* binding strength (Figure 4B).[48-49, 63] However, in a similar fashion, structural defects such as inner cavities are prone to

collapse when exposed to harsh environmental conditions.[187] Those aspects bring forth similar conclusions than those presented for the Fe(II)-N_4 site, *i.e.* that an excess in structural defects or alloying elements would be detrimental for the ORR activity, by 'over-shooting' the optimal OH* binding strength, and that such modified nanostructures would, in addition, show depreciated electrocatalytic activity (**Figure 4B**).

5. Engineering of cathode catalyst layer (CL) for Pt-based and Fe-N-C electrocatalysts and applications in PEFMCs

Although high ORR activity is usually obtained in 3-electrode cell rotating disk electrode (RDE) measurements, the experimental conditions widely differ from those into which the electrocatalysts are meant to operate, *i.e.* PEMFCs, the activities obtained in the latter being far more meaningful than those obtained in liquid electrolyte. In PEMFCs, several challenges arise from the mass transport limitations (*e.g.* O_2 and H^+ transport to the interface, H_2O removal). The ORR in PEFMCs occurs at the triple-phase boundary (catalyst-electrolyte-gas) and involves (i) the electrocatalyst and (ii) H^+, and O_2 circulating through the ionomer and/or the electrode porosities to/from said electrocatalyst and (iii) the provisioning/removal of H_2O.[188] Therefore, apart from the rational design of electrocatalysts with high ORR performance, the engineering of catalytic layers with a well-designed triple-phase boundary is of great importance for practical application, as illustrated in **Figure 5**. First, a good ionomer coverage of the carbon support must be achieved, as to ensure optimal active site accessibility to the charged species. For example, Ott *et al.*[189] modified carbon black surfaces by nitrogen doping,

enhancing the interaction between the ionomer and the carbon surface and leading to an even ionomer coverage, thus significantly reducing the oxygen transport resistance and improving the fuel cell power density for Pt-based electrocatalysts. Likewise, Huang's group [190] also reported the chemical modification of carbon support with surface oxidation, identifying an optimal surface oxygen loading to create favorable carbon-ionomer interaction and to balance hydrophobic and hydrophilic properties on the catalytic layer, favoring the water management. The thickness of the ionomer layer, should also be considered carefully, as Harada *et al.*[191] showed that a dense ionomer layer (> 3 nm) on the top of the active sites resulted in limited local O_2 diffusion. In the presence of Pt-based nanostructures, the interactions between the latter and the ionomer have to be considered, owing to the poisoning of the Pt surface by the side chain of perfluorosulfonated ionomers (*e.g.* $-SO_3^-$).[192] A recent study to address this challenge consisted in depositing a thin layer of carbon (< 1 nm) on the Pt nanoparticles surface to prevent poisoning without compromising gas/proton permeability.[193] Another way to address the Pt poisoning is to optimize the pore structure of the carbon support, which tunes the location of the Pt-based nanoparticles: exposure of the Pt nanoparticles on the carbon support outer surface is favorable, as it eases the O_2 accessibility, but increase the ionomer poisoning effect. Contrarily, the deposition of Pt particles in the carbon inner porosities can efficiently prevent the poisoning effect and particles aggregation during ageing,[194] at the cost of depreciated gas transport (see **Figure 5A**). To this end, Yarlagadda *et al.*[88] identified a perfect trade-off through porous carbon design with a bottleneck pore size of 4 -7 nm, in which Pt particles located inside pore did not suffer

from poisoning by the ionomer (contactless with ionomer) nor high gas transport resistance (**Figure 5A**).

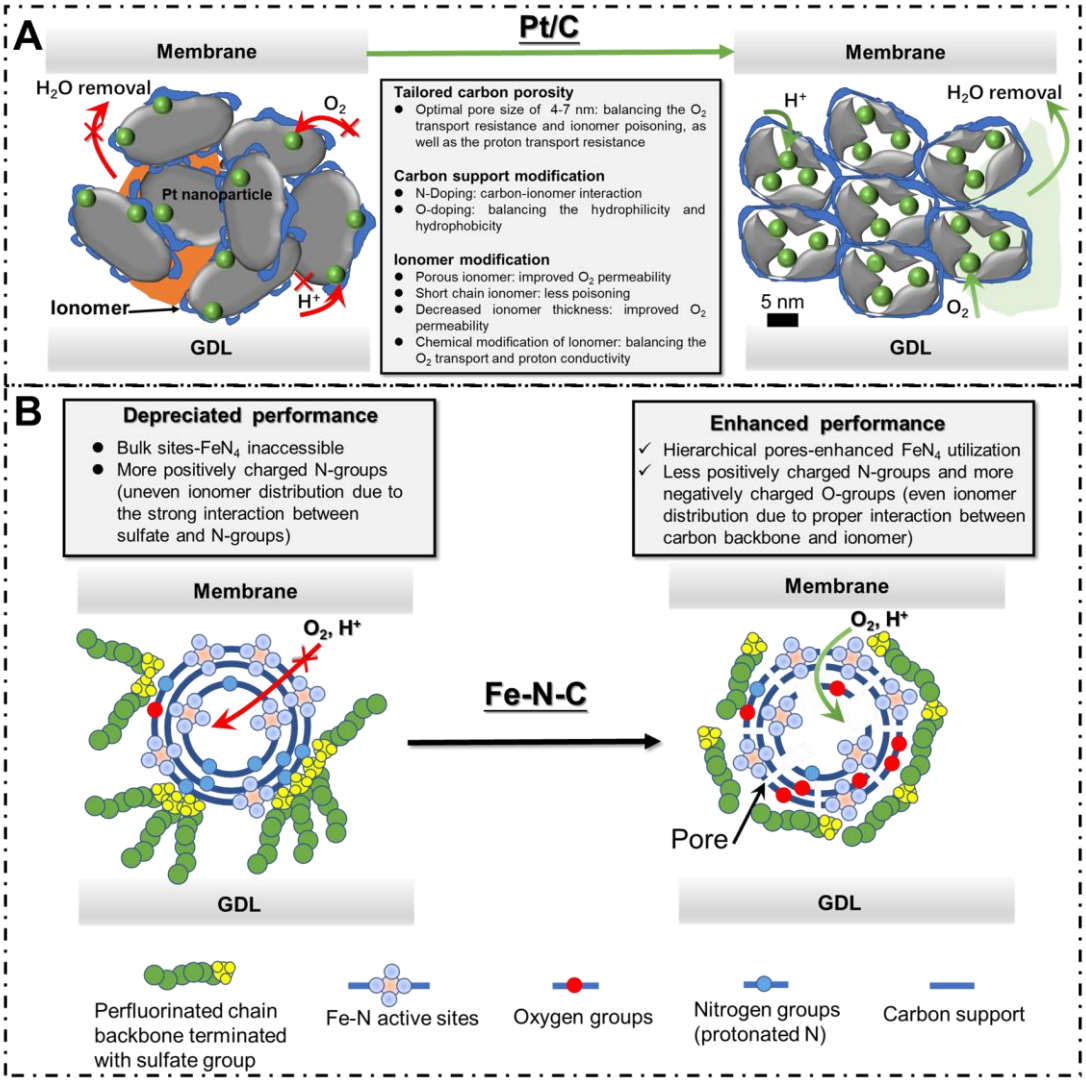

Figure 5. Schematic illustration of cathode catalyst layer and triple-phase boundary engineering on Pt-based (A) and Fe-N-C (B) electrocatalysts.

Inferior intrinsic activity and limited active sites density usually result in thicker catalytic layers for Fe-N-Cs with respect to that of Pt-based catalysts (60-100 μm of CL for Fe-N-Cs *vs.* 10 μm for identical performance for Pt-based catalyst).[195-197] However,

the increased thickness of the Fe-N-Cs catalytic layer not only increases the mass transport limitation,[198] but decreases the utilization of the catalyst located within the catalytic layer and increases the possibility for its detachment and flooding during operation.[196, 199-200] In this end, two strategies are employed for the optimization of Fe-N-Cs performances in PEMFCs as shown in the **Figure 5B**: (1) increasing the accessibility of FeN_4 sites and rationalizing the design of the Fe-N-Cs porous structure. Very recently, Jiao *et al*.[201] proposed an innovative approach to bring the percentage of utilized active sites near 100%, by first pyrolyzing a nanosized zeolitic imidazolate framework (ZIF-8) and then using chemical vapor deposition of $FeCl_3$ to replace the 'vapor-accessible' ZnN_4 moieties originally present in ZIF-8 by FeN_4. An activity in PEMFC of 33 mA/cm_{geo}^2 at 0.9 V(IR-free) was reached, close to target of 2025 set by DOE. The design of an optimized, hierarchical, porous structure would also greatly increase the FeN_4 accessibility, by exposing inaccessible or buried FeN_4 sites, along with favoring the mass transport of reactants and products.[159, 202] However, an overly complex porous network could ultimately be detrimental, by increasing the structure defectivity (thus lowering its stability and compromising the intrinsic activity of FeN_4 sites, see **Figure 4A**) as well as rendering some sites non-accessible to the ionomer; (2) optimizing the catalytic layer structure. Similar to Pt-based systems, the ionomer content plays an important role in facilitating, or limiting, gas transportation and ionic species conductivity. Thus, trade-off between gas transport and proton conductivity should be achieved,[203] in the form of an uniform coverage of the Fe-N-C electrocatalyst by a thin layer of ionomer (< 3 nm).[204] As far as the catalyst-ionomer interactions are concerned, Artyushkova

et al.[205] revealed the pivotal role played by the nitrogen species within the carbon network: the hydrogenated N and positively charged protonated N interact strongly with negatively charged sulfonated groups of perfluorosulfonated ionomers (*e.g.* Nafion®), hence disrupting the ionomer network and limiting the proton transport. On the contrary, surface oxides with a negative charge were deemed responsible for an even distribution of ionomer and optimal interaction between the Fe-N-C and ionomer (**Figure 5B**).

To provide a clear insight into the current state of the Fe-N-Cs as PEMFCs electrocatalysts *vs.* Pt-based systems, a list of some of the most promising Fe-N-Cs and Pt-based systems is provided in **Table 1** and **Table 2**. To allow for a meaningful comparison, the technical details (*e.g.* pressure, gas atmosphere, flow rate, *etc*.) are also provided. It is worth noting that the lack of unified durability test protocols for Fe-N-Cs make the data comparison on that specific aspect meaningless.

Table 1 The MEA-based PEMFC performances of 'state-of-the-art' Fe-N-Cs

Entry[a]	L [b] mg/cm^2	P [c] kPa$_{abs}$	T ^{o}C	FR [d] (H_2/O_2) sccm	RH[e] %	$j_{0.9V}$ [f] O_2 mA/cm^2	P_{max} [g] O_2 mW/cm^2	FR [d] (H_2/Air) sccm	$j_{0.8V}$ [f] Air mA/cm^2	P_{max} [g] Air mW/cm^2	Ref.	Year
DOE	**4.0**	**150**	**80**	-	**100**	**44**	**1000**	-	**150**	**500**	**6**	
S-doped Fe-N-C	4.0	150 (250)	80	200/200	100	-	940* (1030*)	-	-	-	206	2015
Metal Organic Framework (MOF)-derived Fe-N-C	3.5-4.0	150	80	-	100	-	603	-	-	-	207	2015
Polyamide + cyanamide derived Fe-N-C	4.0	100	80	200/200	100	-	870	200/200	90	390*	208	2017
Carbon black + Phenanthroline + polyaniline derived Fe-N-C	4.0	238	80	300/400	100	-	1060*	300/400	120	380*	209	2017
MOF-derived Fe-N-C	2.8	250	80	300/400	100	35*	1141	-	-	-	210	2017
Fe-N-C	2.0	450	80	300/400	100		823*	-	-	-	10	2018

Fe-N-C (50 cm_{geo}^2)	4.0	173	75	-	100	-	750	-	-	570	196	2018
MOF-derived Fe-N-C (pyrolyzed at 700°C under N_2)	4.3	203	80	200/200	100	30	-	200/200	75*	320*	211	2019
MOF-derived, templated Fe-N-C	2.7(O_2) 2.0(Air)	100	80	300/400	100	22	-	300/500	129	420*	159	2019
MOF-derived Fe-N-C	4.0	100	80	200/200	100	-	-	200/200	75*	360*	212	2019
Chemical Vapor Deposition (CVD)-synthesized Fe-N-C	4.0	200	80	300/500	100	27	-	300/500	117*	-	213	2020
MOF-derived Fe-N-C	4.0	200	80	200/200	100	35	750	200/200	64	340*	214	2020
MOF-derived Fe-N-C	4.0	150	80	200/200	100	28.5	-	-	-	-	204	2020
CVD-synthesized Fe-N-C	6.0	150	80	200/1000	100	33	-	500/2000	-	370*	201	2021
MOF-derived, NaCl-assisted Fe-N-C	4.0	100	80	150/200	100	-	890*	150/200	-	390*	215	2021
NH_4Cl-treated Fe-N-C	4.0	150	80	700/1700	100	44.2	-	200/400	151*	601*	17	2022
NH_4Cl-treated + CVD Fe-N-C	4.0	150	80	700/1700	100	33		200/400	85*	535*		
MOF-derived Fe-N-C	3.9	203	80	200/200	100	41.3	>1200	300/1000	199	429	216	2022

[a] DOE: 2025 performance target of department of energy, US; [b] loading of catalyst. [c] total outlet pressure (absolute) for a fully humidified H_2 and O_2/air. [d] flow rate of H_2 and O_2/air. [e] relative humidity. [f] current density (IR-corrected) at applied voltage and gas atmosphere (0.9 V under O_2 or 0.8 V under air). [g] rated power under O_2 or air. * indicates that IR correction is not specified or no IR-correction is applied.

Table 2 The MEA-based PEMFC performances ranking the best among reported Pt-based electrocatalysts

Entry [a]	L [b] mg_{Pt}/cm^2	P [c] kPa_{abs}	T (°C)	FR [d] (H_2/O_2) sccm	RH[e] %	$j_{0.9V}$ [f] O_2 A/mg_{Pt}	$j_{0.9V}$ [f] O_2 mA/cm^2	AST [g] Condition (V)	AST [h] MA(Volt) loss (% or mV)	Ref.	year
DOE	**0.1**	**150**	**80**	**-**	**100**	**0.44**	**44**	**0.6 - 0.95**	**< 40 % < 30 mV**	**6**	
PtNi/C	0.1	150	80		100	0.62	62	0.6 – 1.0	20 %	217	2014
PtNi/C	0.11	150	80	696/1654	65	1.34	147.4	0.6 – 1.3	43% (5000 cycles)	218	2016
Co@Pt/Co-N-C	0.033	150	80	200/200	100	1.08	35.6	0.6 – 1.0	36 % 6 mV	9	2018
Octahedral PtNi/C	0.1	50	80	-	100	0.57	57	-	-	219	2019
PtCo/C	0.1	150	80		100	0.79	79	0.6 – 0.95	37 % 31 mV	220	2019
CoPt/C	0.105	150	80	500/1000	100	0.56	58.8	0.6 – 0.95	19 %	221	2019

[a] DOE: 2025 performance target of department of energy, US; [b] loading of Pt; [c] total outlet pressure (absolute) fully humidified for H_2 and O_2/air; [d] flow rate of H_2 and O_2; [e] relative humidity; [f] current density (IR-corrected) at applied voltage under O_2 (0.9 V); [g] Accelerated stress test (AST) at given potential range according to DOE catalyst durability evaluation protocols [6]; [h] mass activity loss at 0.9 V (IR-corrected), and voltage loss at 0.8 A/cm^2 after 30000 cycles (unless other stated).

In the case of Pt-based catalyst, great accomplishments on both activity and durability have been achieved, even surpassing the performance target set by DOE 2025. (**Table 2**). Hence, it appears that the electrocatalytic performance of Pt-based electrocatalysts is not decisive for the commercial success, the limitations rather arising from the scarcity and cost of platinum, requiring either 100% efficiency in terms of Pt recycling [222] for further utilization or greater advances in terms of catalytic improvement. Although innovative structures far outperforming PtCo have been identified, owing to the directions discussed in Section 3 and 4, translating them from the laboratory-scale to large-scale industry level remains extremely difficult.[66] Fe-N-C electrocatalysts present lower performance with respect to Pt-based electrocatalyst in both activity and durability. The MOF-derived Fe-N-Cs are the most promising, *e.g.* very recently, Wu's group [17] reported a MOF-derived NH_4Cl treated Fe-N-C electrocatalyst that reached the 2025 DOE target in terms of activity (**Table 1**), through the successful implementation of structural defects in the vicinity of the FeN_4 sites. However, those materials showed poor durability (up to 94 % activity loss after 30,000 potential cycles between 0.6 V and open circuit potential). By post-deposition of a N-doped carbon layer onto the Fe-N-C surface, the durability was found to meet the U.S 2025 DOE target, while exhibiting decreased activity. This indicates that both parameters are often correlated, as discussed in Section 4, and that designs that are not bound by the Volcano plot presented

in **Figure 4A** are needed to go 'beyond' those limitations.

By opposition, Fe-N-Cs are better performing than Pt-based electrocatalysts in alkaline environment, as reported in liquid electrolyte [135, 223-225], and beneficiate from the less corrosive environment. This highlights their potential application as anion exchange membrane fuel cells (AEMFCs) cathode electrocatalysts. However, the design of an AEMFC has to consider several challenges that are cathode catalytic layer independent, *i.e.* (i) carbonation is usually encountered in the presence of CO_2 (from the air feed), which dramatically decreases the ionic conductivity of the AEM, the pH and greatly impacts the performances;[226-228] (ii) water management is required to maintain membrane hydration, as water serves as both as a reactant and as a product at the cathode and anode, respectively, while avoiding flooding;[229-231] (iii) the alkaline environment decreases the HOR kinetics at the anode, thus requiring the identification of adapted electrocatalysts for said reaction.[232] As such, the research and development of AEMFCs has lagged far behind the one of PEMFCs. However, recent years have witnessed significant advancements, and high peak power density (*e.g.* > 1 W/cm^2 in H_2/O_2) using Fe-N-C catalysts at the cathode have been reported.[233-236] Specifically, Mustain' group [237] recently developed an AEMFC with a state-of-the-art Fe-N-C electrocatalyst, which achieved a peak power density of > 2 W/cm^2 under H_2/O_2, while > 1 W/cm^2 of power density was still obtained under H_2/Air (CO_2-free).

Here, two critical points were evidenced: (i) the gap between the Pt-based electrocatalysts and Fe-N-C electrocatalysts has been steadily decreasing throughout the years. Fe-N-C are now close to achieve the 2025 DOE target in terms of durability and activity

[17]. The latter has been reached for Pt-based electrocatalysts, and even surpassed (by *ca.* 3 times in terms of $j_{0.9V}$ in A/g^{-1}_{Pt} and mA/cm^{2}_{geo}, see **Table 2**), the main objective being now to even further decrease the Pt content by implementing advanced Pt-based nanostructures in PEMFCs; (ii) hence, for both Fe-N-C and Pt-based electrocatalysts, the transition from liquid electrolyte to PEMFCs is not trivial. Notably, advanced-Pt nanostructures designed around porosity, structural defects or preferential crystallite orientation have yet to be successfully implemented in PEMFCs. The final application should be kept in mind when designing the electrocatalyst, and the iron sites should be excluded from domains where the ionomer/gases cannot access (*e.g.* micropores, *etc*.). The functionalization of the carbon support (or, in the Fe-N-C case, the iron-free moieties) is also pivotal, as it controls the ionomer dispersion over the catalyst layer. Drastically increasing the density of iron sites would be a direction to even further increase the Fe-N-Cs competitiveness, but, as evidenced by Wu's group, obtaining an active and stable Fe-N-C electrocatalyst is extremely challenging. Furthermore, (i) the Fe-N-Cs perform remarkably well in AEMFCs, implying that, owing that the membrane and anode limitations of those systems are addressed, they would be of extreme interest; (ii) M-N-C as supports for Pt-based electrocatalysts have recently encountered interest,[9] in the light of a synergy between the Co@Pt core@shell nanoparticles and a Co-N-C electrocatalyst, the former reducing any H_2O_2 generated on the latter, thus increasing the selectivity, activity and durability while decreasing the Pt loading.

6. Degradation mechanism of Pt-based and Fe-N-C electrocatalysts

As a result of the promises hold by their activity, the durability of Pt-based and Fe-N-C electrocatalysts should be carefully addressed. For both families, at the micrometer scale, the thinning of cathode catalyst layer (the decomposition of carbon support and ionomer) is often observed during ageing, which results in cracking or detachment of the catalytic layer.[196, 238] In consequence, the overall activity suffers a dramatic decrease, especially in the high current region as it is there controlled by the mass transport properties. The catalyst layer corrosion is strongly accelerated by start-up/shut-down events, during which the local heterogeneity on the feed gas concentration also leads to extreme degradation.[239-242] The changes observed at the micrometer scale are direct consequences of phenomena occurring at the atomic/nanometric level, which will be discussed in detail in this section.

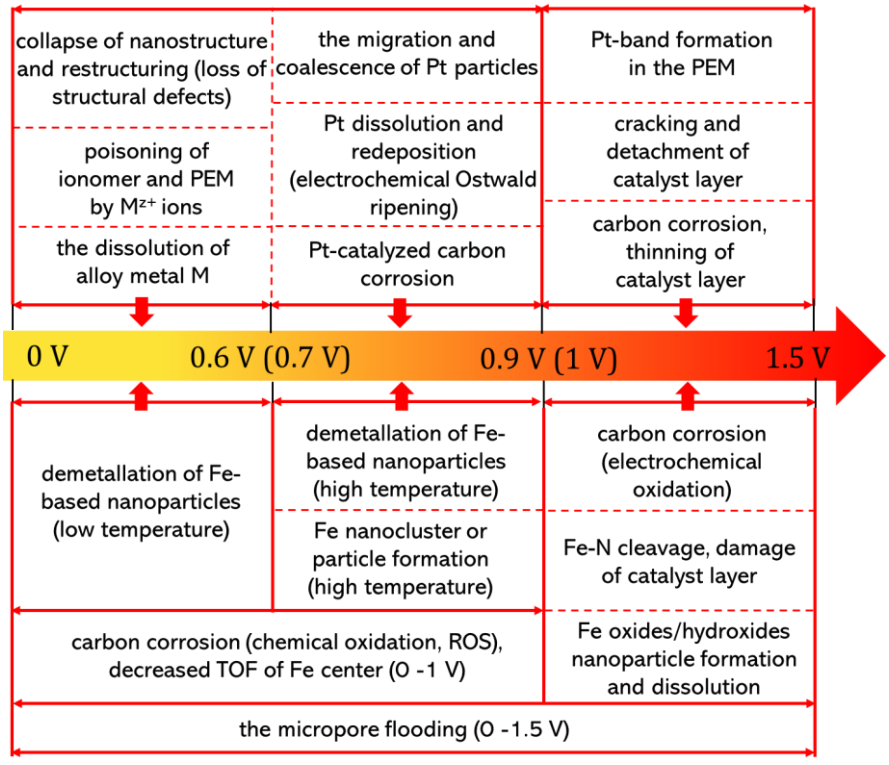

Figure 6. The degradation mechanism of Pt-based (above arrow) and Fe-N-Cs (below arrow) electrocatalysts as a function of potential (given *vs.* RHE).

An overview of the mechanisms as a function of the potential at which the catalytic layer is exposed is presented in **Figure 6**. For Pt-based electrocatalysts, the corrosion of the carbon support occurs in a wide potential range, forming CO/CO_2 or carbon surface oxygen groups.[243] It preferentially occurs on amorphous carbon or carbon-edge defects, thus highlighting the importance of carbon support nature.[244-245] The corrosion rate is significantly enhanced in the presence of Pt nanoparticules.[246] During accelerated stress tests (ASTs) at high potentials (*i.e.* 1.0 – 1.5 V *vs.* RHE, simulating start-up/shut-down events on real PEMFCs operation), the collapse of the carbon structure is observed, impeding mass-transport of reactant gas and water removal from catalyst layer.[247-249] Furthermore, the carbon partial oxidation (*i.e.* generation of surface oxygen groups) also improves the surface hydrophilicity, thus leading to water management issue.[249-250] Besides the carbon support itself degradation, the support corrosion usually induces the loss of electrochemical surface area (ECSA) owing to the detachment of Pt-based nanoparticles and subsequent agglomeration on the support [247, 251] while the crystallite migration and Pt nanoparticle coalescence at high potential was proposed to be dependent on the Pt nanoparticles-support interactions and, especially, to the surface oxygen group coverage. [252]

The dissolution rate of platinum is strongly dependent on the initial particle size, with the smaller ones showing faster dissolution rate compared to the larger ones (Gibbs-Thompson equation).[253] The dissolution phenomenon are usually enhanced at

higher potentials.[254-255]. When exposed to ASTs, the Pt dissolution can be subdivided into anodic scan and cathodic scan dissolution, with the former being less affected by the upper/lower potential limit (UPL/LPL) and showing slower dissolution rate compared to the cathodic sweep. Topalov *et al.*[256] used the place exchange mechanism to justify this phenomenon, with Pt exchanging its place with O at > 1.1 V vs. RHE and being subsequently dissolved during the cathodic scan. It is noteworthy that the Pt^{z+} ions generated from the dissolution of platinum are not only redeposited within catalyst layer, but diffusing into the PEM where Pt^{z+} can be reduced by H_2 crossing-over from anode side, leading to the formation of a Pt-band inside the PEM.[250, 257-259] Crystallite growth is also commonly observed during platinum nanoparticles ageing, and is mainly attributed to (a) the coalescence of nanoparticles and (b) the dissolution of small Pt nanoparticles into Pt^{2+}, followed by redeposition on the larger size Pt nanoparticles (electrochemical Ostwald ripening).[260] The operating conditions (*e.g.* the UPL,[261] relative humidity,[262] temperature,[263] *etc.*) and physicochemical properties of electrocatalyst itself (*e.g.* the initial particles size and shape,[264] pore size distribution,[264] *etc.*) play a crucial role for the stability of Pt nanoparticles during ageing.

PtM/C (M = Co, Ni) suffers from additional ageing mechanisms due to the preferential dissolution of the transition metal during operation.[265] Asset *et al.* [187] emphasized that the lower UPL was crucial to prevent substantial dissolution of Ni, the growth of crystallites size and the loss of structural defects. Sneed *et al.* [266] evidenced that Pt-rich, small size, PtM nanoparticles are stable while larger ones, with higher content of 3d transition metal, are continuously leaching the 3d-transition metal during the operation,

which leads to the formation of hollowed-out shells. This dissolution incidentally leads to the loss of the strain effect induced by the presence of the alloying element,[267-268] although it might under specific ageing conditions, lead to the formation of hollow Pt-rich nanoparticles with enhanced activity.[186] Owing to their smaller initial ECSA (low Pt loading, larger nanostructures), the PtM often exhibit enhanced local O_2 transport resistance, which is magnified during ASTs, thus dramatically decreasing the performance at high current density.[88, 269] The dissolved transition metal M^{z+} cations are not reduced in PEMFCs operation condition, thus still existing as M^{z+} ions in the catalytic layer, [270-271] where they can significantly decrease the proton transport property through strong interaction with the sulfonic acid groups in the perfluorosulfonated membrane and ionomer,[272-273] alongside decreasing the oxygen permeability.[248, 274]

The durability of Fe-N-Cs, especially in PEMFC condition, is far below the target of DOE in 2025 [6] and results of numerous mechanisms. Similarly to Pt, the degradation mechanisms are (i) potential dependent and (ii) chemistry dependent (*e.g.* Fe-based nanoparticle, FeN_xC_y moiety). They include, as illustrated in **Figure 6**, (i) micropore flooding, (ii) demetallation, including the dissolution of Fe-based nanoparticles and disintegration of the FeN_x moiety, (iii) carbon corrosion, including electrochemical oxidation and chemical oxidation. The first mechanism would lead to the "deactivation" of the active sites induced by its inaccessibility to the reactants. Such deactivation might be reversible, through water management or catalyst regeneration, while the latter two result in the "loss" of performance due to destruction of active site (*i.e.* irreversible oxidation of carbon surface and disintegration of FeN_x sites).

Dodelet *et al.*[89, 275] proposed that the electro-oxidation of the carbon transformed the hydrophobic surface to hydrophilic one, which led to easier micropores water flooding where most of the active FeN_x sites were hosted. As such, the micropores water filling impedes the O_2 transport to the FeN_x active sites, along with leading to their demetallation through Le Chatelier principle,[90] inducing dramatic performance drop. Synthesizing the Fe-N-C at high pyrolysis temperature usually lead to an higher graphitization degree and lower heteroatoms doping content, which makes the carbonaceous surface more hydrophobic, hence preventing the flooding.[89]

Demetallation of Fe-N-Cs can be subdivided into (i) dissolution of Fe-based nanoparticles and (ii) disintegration of FeN_x moieties, depending on applied potential and operation temperature in PEMFCs. Choi *et al.*[131] proposed that the demetallation of Fe-based nanoparticles occurred only below 0.7 V *vs*. RHE at low temperature (20 °C), with the potential range extending to 1 V *vs.* RHE at 80 °C.[129] The generated Fe^{2+} can readily diffuse into the membrane and subsequently decrease the proton conductivity. In addition, the presence of Fe^{2+} also leads to a Fenton reaction, favoring the formation of high oxidative radical oxygen species (ROS), which will be discussed in the following paragraphs. The demetallation of Fe-based nanoparticles, *e.g.* low valence Fe metal or iron carbide is also observed at high potential range (*i.e.* above 1 V *vs.* RHE) accompanied with the post-formation of high valence iron compounds (*e.g.* $Fe(OH)_3$).[276] Atomic FeN_xC_y moiety is believed to be highly stable and its destruction mainly occurs at high potential range (*i.e.* 1 V - 1.5 V *vs.* RHE), probably arising from the cleavage of Fe-N bond induced by severe carbon corrosion.[11, 131, 276] The destruction of the FeN_xC_y

moiety generally results in the formation of Fe-based nano-cluster or particles and their subsequent dissolution. Besides, the surface mobility and possible transformations of FeN_xC_y edge and in-plane sites at medium potential range (0.6 - 1 V *vs.* RHE) during ageing at 80 ºC have also been recently reported, resulting in the formation of 2D Fe cluster.[160]

Similar to the case of Pt-based electrocatalysts, carbon corrosion is also prevalent in the Fe-N-Cs during ageing, but it is not catalyzed by the presence of Fe-based moieties. The dramatic carbon support degradation during start-up/shut-down events also holds true, leading to similar consequences (*i.e.* loss of active sites, mass-transport limitation, water management issues). The carbon corrosion is believed to exert more severe effects on the Fe-N-Cs since the active sites (*i.e.* FeN_xC_y) are embedded into carbon matrix and thus are disintegrated with the corrosion of the carbon. The carbon corrosion is also caused by carbon oxidation reaction (COR), which can be classified into two mechanisms, *i.e.* electrochemical oxidation (carbon electrooxidation to CO and CO_2) and chemical oxidation. Choi *et al.*[131] proposed the potential range for CO_2 and CO formation to be above 0.9 V *vs.* RHE at 50 ºC. The COR rate strongly increases at higher temperature/potential.[277] On the other hand, the performance losses during ageing at low potential range (*i.e.* 0.6 V - 1 V *vs*. RHE) are usually governed by chemical oxidation of carbon surface, where the ROS formed from H_2O_2 by the Fenton reaction are responsible for the carbon corrosion. Such oxidation phenomena is particularly true in PEMFC operation condition (O_2 feed, high current density) since the generated amount of H_2O_2 is far higher in comparison to the one detected in an RDE

measurement.[129] Choi *et al*.[278] observed that, although the FeN_xC_y moiety was structurally stable at low potential range, its turnover frequency (TOF) was also dependent of partial chemical carbon oxidation induced by the ROS, which modified the electronic structure of the carbon backbone and, thus, the binding strength of oxygen-based species on the Fe atom center. In addition, CO/CO_2 gas evolution is observed at low potential range (< 0.9 V *vs.* RHE) and the degradation extent is independent of operation temperature and potential range, implying that the chemical oxidation of the carbon surface also plays a vital role in the Fe-N cleavage. Owing to the points aforementioned, it appears that increasing the Fe-N-Cs durability goes through (i) the decrease of Fe-based nanoparticles (to reduce Fe^{2+}-induced membrane poisoning and Fenton reaction); (ii) a highly favored $4e^-$ reactive pathway, to limit the H_2O_2 generation and (iii) an adequate graphitization of the support, to achieve an acceptable trade-off between durability and activity. Interestingly, this last point is not only critical for Fe-N-C electrocatalysts, but also for Pt-based electrocatalysts, as the degradation of the carbon support also leads to the active phase detachment, agglomeration, *etc.* However, going in the direction of highly graphitized supports usually results in low carbon specific surface, *i.e.* low dispersion of the Pt-based nanoparticles and decreased ECSA. Nevertheless, to the advantage of the Fe-N-C electrocatalysts, the carbon-related corrosion ought to be weaker on the latter, owing that a $4e^-$ pathway is favored and Fe-based nanoparticles are removed, since the FeN_x moieties do not catalyze the COR, by opposition to Pt-based nanoparticles.

7. Conclusion and perspectives

Over the past years, considerable progresses have been achieved in developing efficient Pt-based and Fe-N-C electrocatalysts for PEMFCs applications. Here, we compare those two families of electrocatalysts on the basis of (i) their structural properties and ORR mechanism; (ii) their intrinsic ORR activity and (iii) performances in PEMFCs and durability, to assess the potential of Fe-N-Cs are replacement for Pt-based electrocatalysts in PEMFCs applications. Both families of electrocatalysts beneficiate from a wide variety of actives sites and of means to control the latter' activities. Indeed, Pt-based electrocatalysts activity can be finely tuned by the addition of structural defects, alloying elements and/or morphological changes to expose crystallites with preferential orientation, whereas the Fe-N-Cs active site nature, density, localization and carbon backbone defectivity play a crucial role in the electrocatalyst activity and selectivity. For both families of electrocatalysts, the design approaches are currently governed by the Sabatier principle, *i.e.* the reaction is occurring on a given active site (Pt-atom *vs.* FeN_x) that should bound the oxygen intermediate neither too strongly nor too weakly. Hence, they are limited by the scaling relationships between the different oxygen intermediates, which ultimately limits their improvement. Going 'beyond' the top of the volcano plot discussed in Section 4 would require a true paradigm shift in terms of electrocatalyst design, by using, for example, co-catalysis (*i.e.* an ORR mechanism where the different reaction steps are undergone onto different active sites of the electrocatalyst, *e.g.* **evidenced** bi-metallic center for M-N-Cs). Freeing the electrocatalyst design from the scaling relationships is especially crucial for Fe-N-C electrocatalysts,

as the means of tuning their activity (*i.e.* by adding a controlled density of structural defects to modify the d-band of iron) impact their stability. **In the current design landscape, however, the Fe-N-Cs more and more appear as a credible alternative to Pt-based electrocatalysts**, as their performances are now reaching the DOE 2025 target. This point comes with several additional positive features for Fe-N-C electrocatalysts: (i) although still behind for PEMFCs applications, Fe-N-Cs are more interesting than Pt-based electrocatalysts as AEMFCs cathodes; (ii) the Fe-N-Cs, especially in the current economical, and geopolitical context, beneficiate of being only composed of earth-abundant elements, thus being free of the strain that currently exists on the platinum resources; (iii) durability wise, owing that the design of Fe-N-Cs is greatly improved (limitation of the density of actives sites in micropores, removal of the exposed Fe-based nanoparticles, enhanced selectivity for the $4e^-$ pathway, proper graphitization degree), the Fe-N-Cs should exhibit excellent stability in operating ORR conditions, as they should not suffer from Pt-induced carbon corrosion. In conclusion, and considering the challenges related to the implementation of the more complex Pt-based nanostructures in PEMFCs, the Fe-N-Cs hold great promises. However, further improvements in the intrinsic activity should imply new design approaches, as achieving both activity and durability objectives would be challenging by simply moving on the volcano plot branches (see Figure 4). Such new approaches are numerous, ranging from the design of bi-metallic active sites to break the scaling relationships, to functionalizing the carbon backbone with heteroatoms that would not decrease its stability (*e.g.* fluorine[247]) while adequately modifying the iron electronic structure.

Several other points of interest arise from this review, that apply for both Pt-based electrocatalysts and Fe-N-Cs: (i) electrocatalysts should always be designed with the catalytic layer in mind, as numerous promising electrocatalysts cannot be yet implemented in PEMFCs owing to poor ionomer distribution around/within the catalyst, unproper morphology for solid electrolyte applications, *etc*; (ii) especially for Fe-N-Cs, the use of rigorous, and standardized, characterization protocols for the activity and durability is essential, as a proper comparison of those materials stability in their own family, and with Pt-based electrocatalysts, is challenging.

Acknowledgments

C. P.-H. thanks the TRAINER project (Catalysts for Transition to Renewable Energy Future) of the "Make our Planet Great Again" program (Ref. ANR-17-MPGA-0017) for support and S. P. thanks the Institut Carnot MICA (COM-Gra 2020) for support. X. Z. finally would like to thank the China Scholarship Council (CSC) for the PhD grant during his stay at ICPEES.

Author Information

Corresponding Authors *Email: t.asset@unistra.fr; *Email: sergey.pronkin@unistra.fr ; *Email: cuong.pham-huu@unistra.fr

References

(1) Seh, Z. W.; Kibsgaard, J.; Dickens, C. F.; Chorkendorff, I.; Nørskov, J. K.; Jaramillo, T. F., Combining Theory and Experiment in Electrocatalysis: Insights into Materials Design. *Science* **2017,** *355*, eaad4998.

(2) Wan, C.; Duan, X.; Huang, Y., Molecular Design of Single-Atom Catalysts for Oxygen Reduction Reaction. *Adv. Energy Mater.* **2020,** *10*, 1903815-1903833.

(3) Debe, M. K., Electrocatalyst Approaches and Challenges for Automotive Fuel Cells. *Nature* **2012,** *486*, 43-51.

(4) Wu, G.; Zelenay, P., Nanostructured Nonprecious Metal Catalysts for Oxygen Reduction Reaction. *Acc. Chem. Res.* **2013,** *46*, 1878-1889.

(5) Banham, D.; Ye, S., Current Status and Future Development of Catalyst Materials and Catalyst Layers for Proton Exchange Membrane Fuel Cells: An Industrial Perspective. *ACS Energy Lett.* **2017,** *2*, 629-638.

(6) Fuel Cell Technical Team Roadmap. https://www.energy.gov/eere/vehicles/downloads/us-drive-fuel-cell-technical-team-roadmap (accessed 2017).

(7) Huang, X.; Zhao, Z.; Cao, L.; Chen, Y.; Zhu, E.; Lin, Z.; Li, M.; Yan, A.; Zettl, A.; Wang, Y. M.; Duan, X.; Mueller, T.; Huang, Y., High-Performance Transition Metal–Doped Pt_3Ni Octahedra for Oxygen Reduction Reaction. *Science* **2015,** *348*, 1230-1234.

(8) Cui, C.; Gan, L.; Heggen, M.; Rudi, S.; Strasser, P., Compositional Segregation in Shaped Pt Alloy Nanoparticles and Their Structural Behaviour During Electrocatalysis. *Nat. Mater.* **2013,** *12*, 765-771.

(9) Chong, L.; Wen, J.; Kubal, J.; Sen, F. G.; Zou, J.; Greeley, J.; Chan, M.; Barkholtz, H.; Ding, W.; Liu, D.-J., Ultralow-Loading Platinum-Cobalt Fuel Cell Catalysts Derived from Imidazolate Frameworks. *Science* **2018,** *362*, 1276-1281.

(10) Yang, L.; Cheng, D.; Xu, H.; Zeng, X.; Wan, X.; Shui, J.; Xiang, Z.; Cao, D., Unveiling the High-Activity Origin of Single-Atom Iron Catalysts for Oxygen Reduction Reaction. *Proc. Nat. Acad. Sci.* **2018,** *115*, 6626-6631.

(11) Chen, M.; He, Y.; Spendelow, J. S.; Wu, G., Atomically Dispersed Metal Catalysts for Oxygen Reduction. *ACS Energy Lett.* **2019,** *4*, 1619-1633.

(12) Gawande, M. B.; Fornasiero, P.; Zboril, R., Carbon-Based Single-Atom Catalysts for Advanced Applications. *ACS Catal.* **2020,** *10*, 2231-2259.

(13) Jasinski, R., A New Fuel Cell Cathode Catalyst. *Nature* **1964,** *201*, 1212-1213.

(14) Franke, R.; Ohms, D.; Wiesener, K., Investigation of the Influence of Thermal Treatment on the Properties of Carbon Materials Modified by N_4-Chelates for the Reduction of Oxygen in Acidic Media. *J. Electroanal. Chem. Interf. Electrochem.* **1989,** *260*, 63-73.

(15) Gouerec, P.; Savy, M.; Riga, J., Oxygen Reduction in Acidic Media Catalyzed by Pyrolyzed Cobalt Macrocycles Dispersed on an Active Carbon: The Importance of the Content of Oxygen Surface Groups on the Evolution of the Chelate Structure During the Heat Treatment. *Electrochim. Acta* **1998,** *43*, 743-753.

(16) Gupta, S.; Tryk, D.; Bae, I.; Aldred, W.; Yeager, E., Heat-Treated Polyacrylonitrile-Based Catalysts for Oxygen Electroreduction. *J. Appl. Electrochem.* **1989,** *19*, 19-27.

(17) Liu, S.; Li, C.; Zachman, M. J.; Zeng, Y.; Yu, H.; Li, B.; Wang, M.; Braaten, J.; Liu, J.; Meyer III, H. M.; Lucero, M.; Jeremy Kropf, A.; Ercan Alp, E.; Gong, Q.; Shi, Q.; Feng, Z.; Xu, H.; Wang, G.; Myers, D. J.; Xie, J.; Cullen, D. A.; Shawn, L.; Wu, G., Atomically Dispersed Iron Sites with a Nitrogen-Carbon Coating as Highly Active and Durable Oxygen Reduction Catalysts for Fuel Cells. *Nat. Energy*

2022, *7*, 652-663.
(18) Iglesias, D.; Giuliani, A.; Melchionna, M.; Marchesan, S.; Criado, A.; Nasi, L.; Bevilacqua, M.; Tavagnacco, C.; Vizza, F.; Prato, M.; Fornasiero, P., N-Doped Graphitized Carbon Nanohorns as a Forefront Electrocatalyst in Highly Selective O_2 Reduction to H_2O_2. *Chem* **2018,** *4*, 106-123.
(19) Melchionna, M.; Fornasiero, P.; Prato, M., The Rise of Hydrogen Peroxide as the Main Product by Metal-Free Catalysis in Oxygen Reductions. *Adv. Mater.* **2019,** *31*, 1802920-1802924.
(20) Wang, H. F.; Tang, C.; Zhang, Q., A Review of Precious-Metal-Free Bifunctional Oxygen Electrocatalysts: Rational Design and Applications in Zn-Air Batteries. *Adv. Funct. Mater.* **2018,** *28*, 1803329-1803350.
(21) Kulkarni, A.; Siahrostami, S.; Patel, A.; Nørskov, J. K., Understanding Catalytic Activity Trends in the Oxygen Reduction Reaction. *Chem. Rev.* **2018,** *118*, 2302-2312.
(22) Sun, Y.; Silvioli, L.; Sahraie, N. R.; Ju, W.; Li, J.; Zitolo, A.; Li, S.; Bagger, A.; Arnarson, L.; Wang, X.; Moeller, T.; Bernsmeier, D.; Rossmeisl, J.; Jaouen, F.; Strasser, P., Activity-Selectivity Trends in the Electrochemical Production of Hydrogen Peroxide over Single-Site Metal-Nitrogen-Carbon Catalysts. *J. Am. Chem. Soc.* **2019,** *141*, 12372-12381.
(23) Abild-Pedersen, F.; Greeley, J.; Studt, F.; Rossmeisl, J.; Munter, T. R.; Moses, P. G.; Skulason, E.; Bligaard, T.; Nørskov, J. K., Scaling Properties of Adsorption Energies for Hydrogen-Containing Molecules on Transition-Metal Surfaces. *Phys. Rev. Lett.* **2007,** *99*, 016105-016108.
(24) Viswanathan, V.; Hansen, H. A.; Rossmeisl, J.; Nørskov, J. K., Universality in Oxygen Reduction Electrocatalysis on Metal Surfaces. *ACS Catal.* **2012,** *2*, 1654-1660.
(25) Sabatier, P., Hydrogénations Et Déshydrogénations Par Catalyse. *Ber. Dtsch. Chem. Ges.* **1911,** *44*, 1984-2001.
(26) Yan, H.; Xu, B.; Shi, S.; Ouyang, C., First-Principles Study of the Oxygen Adsorption and Dissociation on Graphene and Nitrogen Doped Graphene for Li-Air Batteries. *J. Appl. Phys.* **2012,** *112*, 104316-104320.
(27) Ou, L.; Yang, F.; Liu, Y.; Chen, S., First-Principle Study of the Adsorption and Dissociation of O_2 on Pt (111) in Acidic Media. *J. Phys. Chem. C* **2009,** *113*, 20657-20665.
(28) Liu, K.; Qiao, Z.; Hwang, S.; Liu, Z.; Zhang, H.; Su, D.; Xu, H.; Wu, G.; Wang, G., Mn-and N-Doped Carbon as Promising Catalysts for Oxygen Reduction Reaction: Theoretical Prediction and Experimental Validation. *Appl. Catal. B-Environ.* **2019,** *243*, 195-203.
(29) Janik, M. J.; Taylor, C. D.; Neurock, M., First-Principles Analysis of the Initial Electroreduction Steps of Oxygen over Pt (111). *J. Electrochem. Soc.* **2008,** *156*, B126-B135.
(30) Chen, Y.; Asset, T.; Lee, R.; Artyushkova, K.; Atanassov, P., Kinetic Isotopic Effect Studies of Iron-Nitrogen-Carbon Electrocatalysts for Oxygen Reduction Reaction. *J. Phys. Chem. C* **2019,** *123*, 11476-11483.
(31) Malko, D.; Kucernak, A., Kinetic Isotope Effect in the Oxygen Reduction Reaction (ORR) over Fe-N/C Catalysts under Acidic and Alkaline Conditions. *Electrochem. Commun.* **2017,** *83*, 67-71.
(32) Tse, E. C.; Varnell, J. A.; Hoang, T. T.; Gewirth, A. A., Elucidating Proton Involvement in the Rate-Determining Step for Pt/Pd-Based and Non-Precious-Metal Oxygen Reduction Reaction Catalysts Using the Kinetic Isotope Effect. *J. Phys. Chem. Lett.* **2016,** *7*, 3542-3547.
(33) George, T. Y.; Asset, T.; Avid, A.; Atanassov, P.; Zenyuk, I. V., Kinetic Isotope Effect as a Tool to Investigate the Oxygen Reduction Reaction on Pt-Based Electrocatalysts–Part I: High-Loading Pt/C and Pt Extended Surface. *ChemPhysChem* **2020,** *21*, 469-475.
(34) Rezaei Talarposhti, M.; Asset, T.; Garcia, S. T.; Chen, Y.; Herrera, S.; Dai, S.; Peterson, E. J.;

Artyushkova, K.; Zenyuk, I.; Atanassov, P., Kinetic Isotope Effect as a Tool to Investigate the Oxygen Reduction Reaction on Pt-Based Electrocatalysts–Part II: Effect of Platinum Dispersion. *ChemPhysChem* **2020,** *21*, 1331-1339.
(35) Ramaswamy, N.; Mukerjee, S., Influence of Inner-and Outer-Sphere Electron Transfer Mechanisms During Electrocatalysis of Oxygen Reduction in Alkaline Media. *J. Phys. Chem. C* **2011,** *115*, 18015-18026.
(36) Ramaswamy, N.; Mukerjee, S., Fundamental Mechanistic Understanding of Electrocatalysis of Oxygen Reduction on Pt and Non-Pt Surfaces: Acid Versus Alkaline Media. *Adv. Phys. Chem.* **2012,** *2012*, 491604.
(37) Meng, H.; Jaouen, F.; Proietti, E.; Lefèvre, M.; Dodelet, J.-P., pH-Effect on Oxygen Reduction Activity of Fe-Based Electro-Catalysts. *Electrochem. Commun.* **2009,** *11*, 1986-1989.
(38) Rojas-Carbonell, S.; Artyushkova, K.; Serov, A.; Santoro, C.; Matanovic, I.; Atanassov, P., Effect of pH on the Activity of Platinum Group Metal-Free Catalysts in Oxygen Reduction Reaction. *ACS Catal.* **2018,** *8*, 3041-3053.
(39) Herranz, J.; Jaouen, F.; Lefèvre, M.; Kramm, U. I.; Proietti, E.; Dodelet, J.-P.; Bogdanoff, P.; Fiechter, S.; Abs-Wurmbach, I.; Bertrand, P.; Arruda, T. M.; Mukerjee, S., Unveiling N-Protonation and Anion-Binding Effects on Fe/N/C Catalysts for O_2 Reduction in Proton-Exchange-Membrane Fuel Cells. *J. Phys. Chem. C* **2011,** *115*, 16087-16097.
(40) Zhang, J.; Sasaki, K.; Sutter, E.; Adzic, R., Stabilization of Platinum Oxygen-Reduction Electrocatalysts Using Gold Clusters. *Science* **2007,** *315*, 220-222.
(41) Cui, C.; Gan, L.; Li, H.-H.; Yu, S.-H.; Heggen, M.; Strasser, P., Octahedral PtNi Nanoparticle Catalysts: Exceptional Oxygen Reduction Activity by Tuning the Alloy Particle Surface Composition. *Nano lett.* **2012,** *12*, 5885-5889.
(42) Maciá, M.; Campina, J.; Herrero, E.; Feliu, J., On the Kinetics of Oxygen Reduction on Platinum Stepped Surfaces in Acidic Media. *J. Electroanal. Chem.* **2004,** *564*, 141-150.
(43) Kuzume, A.; Herrero, E.; Feliu, J. M., Oxygen Reduction on Stepped Platinum Surfaces in Acidic Media. *J. Electroanal. Chem.* **2007,** *599*, 333-343.
(44) Gómez-Marín, A. M.; Rizo, R.; Feliu, J. M., Some Reflections on the Understanding of the Oxygen Reduction Reaction at Pt (111). *Beilstein J. Nanotechnol.* **2013,** *4*, 956-967.
(45) Gómez-Marín, A. M.; Feliu, J. M., Oxygen Reduction on Nanostructured Platinum Surfaces in Acidic Media: Promoting Effect of Surface Steps and Ideal Response of Pt (111). *Catal. Today* **2014,** *244*, 172-176.
(46) Bandarenka, A. S.; Hansen, H. A.; Rossmeisl, J.; Stephens, I. E., Elucidating the Activity of Stepped Pt Single Crystals for Oxygen Reduction. *Phys. Chem. Chem. Phys.* **2014,** *16*, 13625-13629.
(47) Shao, M.; Chang, Q.; Dodelet, J.-P.; Chenitz, R., Recent Advances in Electrocatalysts for Oxygen Reduction Reaction. *Chem. Rev.* **2016,** *116*, 3594-3657.
(48) Calle-Vallejo, F.; Tymoczko, J.; Colic, V.; Vu, Q. H.; Pohl, M. D.; Morgenstern, K.; Loffreda, D.; Sautet, P.; Schuhmann, W.; Bandarenka, A. S., Finding Optimal Surface Sites on Heterogeneous Catalysts by Counting Nearest Neighbors. *Science* **2015,** *350*, 185-189.
(49) Le Bacq, O.; Pasturel, A.; Chattot, R.; Previdello, B.; Nelayah, J.; Asset, T.; Dubau, L.; Maillard, F., Effect of Atomic Vacancies on the Structure and the Electrocatalytic Activity of Pt-Rich/C Nanoparticles: A Combined Experimental and Density Functional Theory Study. *ChemCatChem* **2017,** *9*, 2324-2338.
(50) Shao, M.; Peles, A.; Shoemaker, K., Electrocatalysis on Platinum Nanoparticles: Particle Size Effect on Oxygen Reduction Reaction Activity. *Nano lett.* **2011,** *11*, 3714-3719.

(51) Perez-Alonso, F. J.; McCarthy, D. N.; Nierhoff, A.; Hernandez-Fernandez, P.; Strebel, C.; Stephens, I. E.; Nielsen, J. H.; Chorkendorff, I., The Effect of Size on the Oxygen Electroreduction Activity of Mass-Selected Platinum Nanoparticles. *Angew. Chem., Int. Ed.* **2012,** *51*, 4641-4643.
(52) Liu, J.; Jiao, M.; Mei, B.; Tong, Y.; Li, Y.; Ruan, M.; Song, P.; Sun, G.; Jiang, L.; Wang, Y.; Jiang, Z.; Gu, L.; Zhou, Z.; Xu, W., Carbon-Supported Divacancy-Anchored Platinum Single-Atom Electrocatalysts with Superhigh Pt Utilization for the Oxygen Reduction Reaction. *Angew. Chem. Int. Ed.* **2019,** *131*, 1175-1179.
(53) Liu, J.; Bak, J.; Roh, J.; Lee, K.-S.; Cho, A.; Han, J. W.; Cho, E., Reconstructing the Coordination Environment of Platinum Single-Atom Active Sites for Boosting Oxygen Reduction Reaction. *ACS Catal.* **2020,** *11*, 466-475.
(54) Greeley, J.; Stephens, I.; Bondarenko, A.; Johansson, T. P.; Hansen, H. A.; Jaramillo, T.; Rossmeisl, J.; Chorkendorff, I.; Nørskov, J. K., Alloys of Platinum and Early Transition Metals as Oxygen Reduction Electrocatalysts. *Nat. Chem.* **2009,** *1*, 552-556.
(55) Escudero-Escribano, M.; Malacrida, P.; Hansen, M. H.; Vej-Hansen, U. G.; Velázquez-Palenzuela, A.; Tripkovic, V.; Schiøtz, J.; Rossmeisl, J.; Stephens, I. E.; Chorkendorff, I., Tuning the Activity of Pt Alloy Electrocatalysts by Means of the Lanthanide Contraction. *Science* **2016,** *352*, 73-76.
(56) Colic, V.; Bandarenka, A. S., Pt Alloy Electrocatalysts for the Oxygen Reduction Reaction: From Model Surfaces to Nanostructured Systems. *ACS Catal.* **2016,** *6*, 5378-5385.
(57) Strasser, P.; Koh, S.; Anniyev, T.; Greeley, J.; More, K.; Yu, C.; Liu, Z.; Kaya, S.; Nordlund, D.; Ogasawara, H.; Toney, M. F.; Nilsson, A., Lattice-Strain Control of the Activity in Dealloyed Core-Shell Fuel Cell Catalysts. *Nat. Chem.* **2010,** *2*, 454-460.
(58) Mavrikakis, M.; Hammer, B.; Nørskov, J. K., Effect of Strain on the Reactivity of Metal Surfaces. *Phys. Rev. Lett.* **1998,** *81*, 2819-2822.
(59) Tian, X.; Zhao, X.; Su, Y.-Q.; Wang, L.; Wang, H.; Dang, D.; Chi, B.; Liu, H.; Hensen, E. J.; Lou, X. W. D.; Xia, B. Y., Engineering Bunched Pt-Ni Alloy Nanocages for Efficient Oxygen Reduction in Practical Fuel Cells. *Science* **2019,** *366*, 850-856.
(60) Wang, L.; Zeng, Z.; Gao, W.; Maxson, T.; Raciti, D.; Giroux, M.; Pan, X.; Wang, C.; Greeley, J., Tunable Intrinsic Strain in Two-Dimensional Transition Metal Electrocatalysts. *Science* **2019,** *363*, 870-874.
(61) Asset, T.; Chattot, R.; Fontana, M.; Mercier-Guyon, B.; Job, N.; Dubau, L.; Maillard, F., A Review on Recent Developments and Prospects for the Oxygen Reduction Reaction on Hollow Pt-Alloy Nanoparticles. *ChemPhysChem* **2018,** *19*, 1552-1567.
(62) Chattot, R.; Asset, T.; Bordet, P.; Drnec, J.; Dubau, L.; Maillard, F., Beyond Strain and Ligand Effects: Microstrain-Induced Enhancement of the Oxygen Reduction Reaction Kinetics on Various PtNi/C Nanostructures. *ACS Catal.* **2017,** *7*, 398-408.
(63) Chattot, R.; Le Bacq, O.; Beermann, V.; Kühl, S.; Herranz, J.; Henning, S.; Kühn, L.; Asset, T.; Guétaz, L.; Renou, G.; Drnec, J.; Bordet, P.; Pasturel, A.; Eychmuller, A.; Schmidt, T. J.; Strasser, P.; Dubau, L.; Maillard, F., Surface Distortion as a Unifying Concept and Descriptor in Oxygen Reduction Reaction Electrocatalysis. *Nat. Mater.* **2018,** *17*, 827-833.
(64) Zhang, L.; Roling, L. T.; Wang, X.; Vara, M.; Chi, M.; Liu, J.; Choi, S.-I.; Park, J.; Herron, J. A.; Xie, Z.; Mavrikakis, M.; Xia, Y., Platinum-Based Nanocages with Subnanometer-Thick Walls and Well-Defined, Controllable Facets. *Science* **2015,** *349*, 412-416.
(65) Wang, C.; Daimon, H.; Lee, Y.; Kim, J.; Sun, S., Synthesis of Monodisperse Pt Nanocubes and Their Enhanced Catalysis for Oxygen Reduction. *J. Am. Chem. Soc.* **2007,** *129*, 6974-6975.

(66) Ly, A.; Asset, T.; Atanassov, P., Integrating Nanostructured Pt-Based Electrocatalysts in Proton Exchange Membrane Fuel Cells. *J. Power Sources* **2020,** *478*, 228516-228524.
(67) Kneebone, J. L.; Daifuku, S. L.; Kehl, J. A.; Wu, G.; Chung, H. T.; Hu, M. Y.; Alp, E. E.; More, K. L.; Zelenay, P.; Holby, E. F.; Neidig, M. L., A Combined Probe-Molecule, Mössbauer, Nuclear Resonance Vibrational Spectroscopy, and Density Functional Theory Approach for Evaluation of Potential Iron Active Sites in an Oxygen Reduction Reaction Catalyst. *J. Phys. Chem. C* **2017,** *121*, 16283-16290.
(68) Zitolo, A.; Goellner, V.; Armel, V.; Sougrati, M.-T.; Mineva, T.; Stievano, L.; Fonda, E.; Jaouen, F., Identification of Catalytic Sites for Oxygen Reduction in Iron-and Nitrogen-Doped Graphene Materials. *Nat. Mater.* **2015,** *14*, 937-942.
(69) Li, Y.; Liu, X.; Zheng, L.; Shang, J.; Wan, X.; Hu, R.; Guo, X.; Hong, S.; Shui, J., Preparation of Fe-N-C Catalysts with FeN_x (X= 1, 3, 4) Active Sites and Comparison of Their Activities for the Oxygen Reduction Reaction and Performances in Proton Exchange Membrane Fuel Cells. *J. Mater. Chem. A* **2019,** *7*, 26147-26153.
(70) Shen, H.; Gracia-Espino, E.; Ma, J.; Tang, H.; Mamat, X.; Wagberg, T.; Hu, G.; Guo, S., Atomically FeN_2 Moieties Dispersed on Mesoporous Carbon: A New Atomic Catalyst for Efficient Oxygen Reduction Catalysis. *Nano Energy* **2017,** *35*, 9-16.
(71) Lefèvre, M.; Dodelet, J.-P., Fe-Based Catalysts for the Reduction of Oxygen in Polymer Electrolyte Membrane Fuel Cell Conditions: Determination of the Amount of Peroxide Released During Electroreduction and Its Influence on the Stability of the Catalysts. *Electrochim. Acta* **2003,** *48*, 2749-2760.
(72) Lefèvre, M.; Dodelet, J.; Bertrand, P., Molecular Oxygen Reduction in PEM Fuel Cells: Evidence for the Simultaneous Presence of Two Active Sites in Fe-Based Catalysts. *J. Phys. Chem. B* **2002,** *106*, 8705-8713.
(73) Zhu, C.; Shi, Q.; Xu, B. Z.; Fu, S.; Wan, G.; Yang, C.; Yao, S.; Song, J.; Zhou, H.; Du, D.; Beckman, S. P.; Su, D.; Lin, Y., Hierarchically Porous M-N-C (M = Co and Fe) Single-Atom Electrocatalysts with Robust MN_x Active Moieties Enable Enhanced ORR Performance. *Adv. Energy Mater.* **2018,** *8*, 1801956-1801963.
(74) Kabir, S.; Artyushkova, K.; Kiefer, B.; Atanassov, P., Computational and Experimental Evidence for a New TM-N_3/C Moiety Family in Non-PGM Electrocatalysts. *Phys. Chem. Chem. Phys.* **2015,** *17*, 17785-17789.
(75) Holby, E. F.; Wu, G.; Zelenay, P.; Taylor, C. D., Structure of Fe–N_x–C Defects in Oxygen Reduction Reaction Catalysts from First-Principles Modeling. *J. Phys. Chem. C* **2014,** *118*, 14388-14393.
(76) Liu, J.; Gong, Z.; Allen, C.; Ge, W.; Gong, H.; Liao, J.; Liu, J.; Huang, K.; Yan, M.; Liu, R.; He, G.; Dong, J.; Ye, G.; Fei, H., Edge-Hosted Fe-N_3 Sites on a Multiscale Porous Carbon Framework Combining High Intrinsic Activity with Efficient Mass Transport for Oxygen Reduction. *Chem Catal.* **2021,** *1*, 1291-1307.
(77) Liang, X.; Li, Z.; Xiao, H.; Zhang, T.; Xu, P.; Zhang, H.; Gao, Q.; Zheng, L., Two Types of Single-Atom FeN_4 and FeN_5 Electrocatalytic Active Centers on N-Doped Carbon Driving High Performance of the SA-Fe-NC Oxygen Reduction Reaction Catalyst. *Chem. Mater.* **2021,** *33*, 5542-5554.
(78) Lai, Q.; Zheng, L.; Liang, Y.; He, J.; Zhao, J.; Chen, J., Metal-Organic-Framework-Derived Fe-N/C Electrocatalyst with Five-Coordinated Fe-N_x Sites for Advanced Oxygen Reduction in Acid Media. *ACS Catal.* **2017,** *7*, 1655-1663.
(79) Kramm, U. I.; Herranz, J.; Larouche, N.; Arruda, T. M.; Lefèvre, M.; Jaouen, F.; Bogdanoff, P.; Fiechter, S.; Abs-Wurmbach, I.; Mukerjee, S.; Dodelet, J.-P., Structure of the Catalytic Sites in Fe/N/C-

Catalysts for O_2-Reduction in PEM Fuel Cells. *Phys. Chem. Chem. Phys.* **2012,** *14*, 11673-11688.
(80) Kramm, U. I.; Lefèvre, M.; Larouche, N.; Schmeisser, D.; Dodelet, J.-P., Correlations between Mass Activity and Physicochemical Properties of Fe/N/C Catalysts for the ORR in PEM Fuel Cell Via ^{57}Fe Mössbauer Spectroscopy and Other Techniques. *J. Am. Chem. Soc.* **2014,** *136*, 978-985.
(81) Zhu, Y.; Zhang, B.; Liu, X.; Wang, D. W.; Su, D. S., Unravelling the Structure of Electrocatalytically Active Fe–N Complexes in Carbon for the Oxygen Reduction Reaction. *Angew. Chem., Int. Ed.* **2014,** *126*, 10849-10853.
(82) Liu, W.; Zhang, L.; Liu, X.; Liu, X.; Yang, X.; Miao, S.; Wang, W.; Wang, A.; Zhang, T., Discriminating Catalytically Active FeN_x Species of Atomically Dispersed Fe-N-C Catalyst for Selective Oxidation of the C-H Bond. *J. Am. Chem. Soc.* **2017,** *139*, 10790-10798.
(83) Asset, T.; Atanassov, P., Iron-Nitrogen-Carbon Catalysts for Proton Exchange Membrane Fuel Cells. *Joule* **2020,** *4*, 33-44.
(84) Liu, Q.; Li, Q.; Chen, S., Metal–Nitrogen Coordination Moieties in Carbon for Effective Electrocatalytic Reduction of Oxygen. *Curr. Opin. Electrochem.* **2020,** *21*, 46-54.
(85) Li, J.; Sougrati, M. T.; Zitolo, A.; Ablett, J. M.; Oğuz, I. C.; Mineva, T.; Matanovic, I.; Atanassov, P.; Huang, Y.; Zenyuk, I.; Di Cicco, A.; Kumar, K.; Dubau, L.; Maillard, F.; Drazic, G.; Jaouen, F., Identification of Durable and Non-Durable FeN_x Sites in Fe-N-C Materials for Proton Exchange Membrane Fuel Cells. *Nat. Catal.* **2021,** *4*, 10-19.
(86) Kramm, U. I.; Ni, L.; Wagner, S., ^{57}Fe Mössbauer Spectroscopy Characterization of Electrocatalysts. *Adv. Mater.* **2019,** *31*, 1805623-1805633.
(87) Lefèvre, M.; Proietti, E.; Jaouen, F.; Dodelet, J.-P., Iron-Based Catalysts with Improved Oxygen Reduction Activity in Polymer Electrolyte Fuel Cells. *science* **2009,** *324*, 71-74.
(88) Yarlagadda, V.; Carpenter, M. K.; Moylan, T. E.; Kukreja, R. S.; Koestner, R.; Gu, W.; Thompson, L.; Kongkanand, A., Boosting Fuel Cell Performance with Accessible Carbon Mesopores. *ACS Energy Lett.* **2018,** *3*, 618-621.
(89) Yang, L.; Larouche, N.; Chenitz, R.; Zhang, G.; Lefèvre, M.; Dodelet, J.-P., Activity, Performance, and Durability for the Reduction of Oxygen in PEM Fuel Cells, of Fe/N/C Electrocatalysts Obtained from the Pyrolysis of Metal-Organic-Framework and Iron Porphyrin Precursors. *Electrochim. Acta* **2015,** *159*, 184-197.
(90) Chenitz, R.; Kramm, U. I.; Lefèvre, M.; Glibin, V.; Zhang, G.; Sun, S.; Dodelet, J.-P., A Specific Demetalation of Fe-N_4 Catalytic Sites in the Micropores of NC_Ar+NH_3 Is at the Origin of the Initial Activity Loss of the Highly Active Fe/N/C Catalyst Used for the Reduction of Oxygen in PEM Fuel Cells. *Energy Environ. Sci.* **2018,** *11*, 365-382.
(91) Li, J.; Ghoshal, S.; Liang, W.; Sougrati, M.-T.; Jaouen, F.; Halevi, B.; McKinney, S.; McCool, G.; Ma, C.; Yuan, X.; Ma, Z.-F.; Mukerjee, S.; Qingying, J., Structural and Mechanistic Basis for the High Activity of Fe-N-C Catalysts toward Oxygen Reduction. *Energy Environ. Sci.* **2016,** *9*, 2418-2432.
(92) Jia, Q.; Ramaswamy, N.; Tylus, U.; Strickland, K.; Li, J.; Serov, A.; Artyushkova, K.; Atanassov, P.; Anibal, J.; Gumeci, C.; Barton, S. C.; Sougrati, M. T.; Jaouen, F.; Halevi, B.; Mukerjee, S., Spectroscopic Insights into the Nature of Active Sites in Iron-Nitrogen-Carbon Electrocatalysts for Oxygen Reduction in Acid. *Nano Energy* **2016,** *29*, 65-82.
(93) Jia, Q.; Ramaswamy, N.; Hafiz, H.; Tylus, U.; Strickland, K.; Wu, G.; Barbiellini, B.; Bansil, A.; Holby, E. F.; Zelenay, P. M., Sanjeev, Experimental Observation of Redox-Induced Fe-N Switching Behavior as a Determinant Role for Oxygen Reduction Activity. *ACS nano* **2015,** *9*, 12496-12505.
(94) Li, J.; Alsudairi, A.; Ma, Z.-F.; Mukerjee, S.; Jia, Q., Asymmetric Volcano Trend in Oxygen

Reduction Activity of Pt and Non-Pt Catalysts: In Situ Identification of the Site-Blocking Effect. *J. Am. Chem. Soc.* **2017,** *139*, 1384-1387.
(95) Xiao, M.; Zhu, J.; Ma, L.; Jin, Z.; Ge, J.; Deng, X.; Hou, Y.; He, Q.; Li, J.; Jia, Q.; Mukerjee, S.; Yang, R.; Jiang, Z.; Su, D.; Liu, C.; Xing, W., Microporous Framework Induced Synthesis of Single-Atom Dispersed Fe-NC Acidic ORR Catalyst and Its in Situ Reduced Fe-N_4 Active Site Identification Revealed by X-Ray Absorption Spectroscopy. *ACS Catal.* **2018,** *8*, 2824-2832.
(96) Osmieri, L.; Ahluwalia, R. K.; Wang, X.; Chung, H. T.; Yin, X.; Kropf, A. J.; Park, J.; Cullen, D. A.; More, K. L.; Zelenay, P.; Myers, D. J.; Neyerlin, K. C., Elucidation of Fe-NC Electrocatalyst Active Site Functionality Via in-Situ X-Ray Absorption and Operando Determination of Oxygen Reduction Reaction Kinetics in a PEFC. *Appl. Catal. B: Environ.* **2019,** *257*, 117929-117941.
(97) Charreteur, F.; Jaouen, F.; Ruggeri, S.; Dodelet, J.-P., Fe/N/C Non-Precious Catalysts for PEM Fuel Cells: Influence of the Structural Parameters of Pristine Commercial Carbon Blacks on Their Activity for Oxygen Reduction. *Electrochim. Acta* **2008,** *53*, 2925-2938.
(98) Jaouen, F.; Herranz, J.; Lefevre, M.; Dodelet, J.-P.; Kramm, U. I.; Herrmann, I.; Bogdanoff, P.; Maruyama, J.; Nagaoka, T.; Garsuch, A.; Dahn, J. R.; Olson, T.; Pylypenko, S.; Atanassov, P.; Ustinov, E. A., Cross-Laboratory Experimental Study of Non-Noble-Metal Electrocatalysts for the Oxygen Reduction Reaction. *ACS Appl. Mater. Interfaces* **2009,** *1*, 1623-1639.
(99) Liu, K.; Wu, G.; Wang, G., Role of Local Carbon Structure Surrounding FeN_4 Sites in Boosting the Catalytic Activity for Oxygen Reduction. *J. Phys. Chem. C* **2017,** *121*, 11319-11324.
(100) Mineva, T.; Matanovic, I.; Atanassov, P.; Sougrati, M.-T.; Stievano, L.; Clémancey, M.; Kochem, A.; Latour, J.-M.; Jaouen, F., Understanding Active Sites in Pyrolyzed Fe-N-C Catalysts for Fuel Cell Cathodes by Bridging Density Functional Theory Calculations and ^{57}Fe Mössbauer Spectroscopy. *ACS Catal.* **2019,** *9*, 9359-9371.
(101) Li, J.; Jaouen, F., Structure and Activity of Metal-Centered Coordination Sites in Pyrolyzed Metal-Nitrogen-Carbon Catalysts for the Electrochemical Reduction of O_2. *Curr. Opin. Electrochem.* **2018,** *9*, 198-206.
(102) Workman, M. J.; Serov, A.; Tsui, L.-k.; Atanassov, P.; Artyushkova, K., Fe-N-C Catalyst Graphitic Layer Structure and Fuel Cell Performance. *ACS Energy Lett.* **2017,** *2*, 1489-1493.
(103) Serov, A.; Artyushkova, K.; Atanassov, P., Fe-N-C Oxygen Reduction Fuel Cell Catalyst Derived from Carbendazim: Synthesis, Structure, and Reactivity. *Adv. Energy Mater.* **2014,** *4*, 1301735-1301741.
(104) Kim, S.-J.; Mahmood, J.; Kim, C.; Han, G.-F.; Kim, S.-W.; Jung, S.-M.; Zhu, G.; De Yoreo, J. J.; Kim, G.; Baek, J.-B., Defect-Free Encapsulation of Fe^0 in 2D Fused Organic Networks as a Durable Oxygen Reduction Electrocatalyst. *J. Am. Chem. Soc.* **2018,** *140*, 1737-1742.
(105) Lou, Y.; Liu, J.; Liu, M.; Wang, F., Hexagonal Fe_2N Coupled with N-Doped Carbon: Crystal-Plane-Dependent Electrocatalytic Activity for Oxygen Reduction. *ACS Catal.* **2020,** *10*, 2443-2451.
(106) Su, Y.; Jiang, H.; Zhu, Y.; Yang, X.; Shen, J.; Zou, W.; Chen, J.; Li, C., Enriched Graphitic N-Doped Carbon-Supported Fe_3O_4 Nanoparticles as Efficient Electrocatalysts for Oxygen Reduction Reaction. *J. Mater. Chem. A* **2014,** *2*, 7281-7287.
(107) Ren, G.; Lu, X.; Li, Y.; Zhu, Y.; Dai, L.; Jiang, L., Porous Core-Shell Fe_3C Embedded N-Doped Carbon Nanofibers as an Effective Electrocatalysts for Oxygen Reduction Reaction. *ACS Appl. Mater. Interfaces* **2016,** *8*, 4118-4125.
(108) Wu, Z.-S.; Yang, S.; Sun, Y.; Parvez, K.; Feng, X.; Mullen, K., 3D Nitrogen-Doped Graphene Aerogel-Supported Fe_3O_4 Nanoparticles as Efficient Electrocatalysts for the Oxygen Reduction Reaction. *J. Am. Chem. Soc.* **2012,** *134*, 9082-9085.

(109) Vij, V.; Tiwari, J. N.; Lee, W.-G.; Yoon, T.; Kim, K. S., Hemoglobin-Carbon Nanotube Derived Noble-Metal-Free Fe_5C_2-Based Catalyst for Highly Efficient Oxygen Reduction Reaction. *Sci. Rep.* **2016,** *6*, 1-8.
(110) Xiao, J.; Xu, Y.; Xia, Y.; Xi, J.; Wang, S., Ultra-Small Fe_2N Nanocrystals Embedded into Mesoporous Nitrogen-Doped Graphitic Carbon Spheres as a Highly Active, Stable, and Methanol-Tolerant Electrocatalyst for the Oxygen Reduction Reaction. *Nano Energy* **2016,** *24*, 121-129.
(111) Chung, H. T.; Won, J. H.; Zelenay, P., Active and Stable Carbon Nanotube/Nanoparticle Composite Electrocatalyst for Oxygen Reduction. *Nat. Commun.* **2013,** *4*, 1-5.
(112) Ao, X.; Zhang, W.; Li, Z.; Li, J.-G.; Soule, L.; Huang, X.; Chiang, W.-H.; Chen, H. M.; Wang, C.; Liu, M.; Zeng, X. C., Markedly Enhanced Oxygen Reduction Activity of Single-Atom Fe Catalysts Via Integration with Fe Nanoclusters. *ACS nano* **2019,** *13*, 11853-11862.
(113) Ao, X.; Zhang, W.; Li, Z.; Lv, L.; Ruan, Y.; Wu, H.-H.; Chiang, W.-H.; Wang, C.; Liu, M.; Zeng, X. C., Unraveling the High-Activity Nature of Fe-N-C Electrocatalysts for the Oxygen Reduction Reaction: The Extraordinary Synergy between $Fe\text{-}N_4$ and Fe_4N. *J. Mater. Chem. A* **2019,** *7*, 11792-11801.
(114) Lv, M.; Guo, H.; Shen, H.; Wang, J.; Wang, J.; Shimakawa, Y.; Yang, M., Fe_3C Cluster-Promoted Single-Atom Fe, N Doped Carbon for Oxygen-Reduction Reaction. *Phys. Chem. Chem. Phys.* **2020,** *22*, 7218-7223.
(115) Li, Z.; Wei, L.; Jiang, W.-J.; Hu, Z.; Luo, H.; Zhao, W.; Xu, T.; Wu, W.; Wu, M.; Hu, J.-S., Chemical State of Surrounding Iron Species Affects the Activity of $Fe\text{-}N_x$ for Electrocatalytic Oxygen Reduction. *Appl. Catal. B: Environ.* **2019,** *251*, 240-246.
(116) Zhou, F.; Yu, P.; Sun, F.; Zhang, G.; Liu, X.; Wang, L., The Cooperation of Fe_3C Nanoparticles with Isolated Single Iron Atoms to Boost the Oxygen Reduction Reaction for Zn–Air Batteries. *J. Mater. Chem. A* **2021,** *9*, 6831-6840.
(117) Hu, S.; Ni, W.; Yang, D.; Ma, C.; Zhang, J.; Duan, J.; Gao, Y.; Zhang, S., Fe_3O_4 Nanoparticles Encapsulated in Single-Atom Fe-N-C Towards Efficient Oxygen Reduction Reaction: Effect of the Micro and Macro Pores. *Carbon* **2020,** *162*, 245-255.
(118) Zhang, C.; Liu, J.; Ye, Y.; Aslam, Z.; Brydson, R.; Liang, C., Fe-N-Doped Mesoporous Carbon with Dual Active Sites Loaded on Reduced Graphene Oxides for Efficient Oxygen Reduction Catalysts. *ACS Appl. Mater. Interfaces* **2018,** *10*, 2423-2429.
(119) Sun, X.; Wei, P.; Gu, S.; Zhang, J.; Jiang, Z.; Wan, J.; Chen, Z.; Huang, L.; Xu, Y.; Fang, C.; Li, Q.; Han, J.; Huang, Y., Atomic-Level Fe-N-C Coupled with Fe_3C-Fe Nanocomposites in Carbon Matrixes as High-Efficiency Bifunctional Oxygen Catalysts. *Small* **2020,** *16*, 1906057-1906066.
(120) Li, L.; Li, Y.; Xiao, Y.; Zeng, R.; Tang, X.; Yang, W.; Huang, J.; Yuan, K.; Chen, Y., Fe_3O_4-Encapsulating N-Doped Porous Carbon Materials as Efficient Oxygen Reduction Reaction Electrocatalysts for Zn–Air Batteries. *Chem. Commun.* **2019,** *55*, 7538-7541.
(121) Jiang, W.-J.; Gu, L.; Li, L.; Zhang, Y.; Zhang, X.; Zhang, L.-J.; Wang, J.-Q.; Hu, J.-S.; Wei, Z.; Wan, L.-J., Understanding the High Activity of Fe-N-C Electrocatalysts in Oxygen Reduction: Fe/Fe_3C Nanoparticles Boost the Activity of $Fe\text{-}N_x$. *J. Am. Chem. Soc.* **2016,** *138*, 3570-3578.
(122) Wu, G.; More, K. L.; Johnston, C. M.; Zelenay, P., High-Performance Electrocatalysts for Oxygen Reduction Derived from Polyaniline, Iron, and Cobalt. *Science* **2011,** *332*, 443-447.
(123) Varnell, J. A.; Edmund, C.; Schulz, C. E.; Fister, T. T.; Haasch, R. T.; Timoshenko, J.; Frenkel, A. I.; Gewirth, A. A., Identification of Carbon-Encapsulated Iron Nanoparticles as Active Species in Non-Precious Metal Oxygen Reduction Catalysts. *Nat. Commun.* **2016,** *7*, 1-9.
(124) Strickland, K.; Miner, E.; Jia, Q.; Tylus, U.; Ramaswamy, N.; Liang, W.; Sougrati, M.-T.; Jaouen,

F.; Mukerjee, S., Highly Active Oxygen Reduction Non-Platinum Group Metal Electrocatalyst without Direct Metal-Nitrogen Coordination. *Nat. Commun.* **2015,** *6*, 1-8.
(125) Deng, D.; Yu, L.; Chen, X.; Wang, G.; Jin, L.; Pan, X.; Deng, J.; Sun, G.; Bao, X., Iron Encapsulated within Pod-Like Carbon Nanotubes for Oxygen Reduction Reaction. *Angew. Chem., Int. Ed.* **2013,** *125*, 389-393.
(126) Wang, K.; Chen, H.; Zhang, X.; Tong, Y.; Song, S.; Tsiakaras, P.; Wang, Y., Iron Oxide@Graphitic Carbon Core-Shell Nanoparticles Embedded in Ordered Mesoporous N-Doped Carbon Matrix as an Efficient Cathode Catalyst for PEMFC. *Appl. Catal. B: Environ.* **2020,** *264*, 118468-118478.
(127) Qiao, Y.; Yuan, P.; Hu, Y.; Zhang, J.; Mu, S.; Zhou, J.; Li, H.; Xia, H.; He, J.; Xu, Q., Sulfuration of an Fe-N-C Catalyst Containing Fe_xC/Fe Species to Enhance the Catalysis of Oxygen Reduction in Acidic Media and for Use in Flexible Zn–Air Batteries. *Adv. Mater.* **2018,** *30*, 1804504-1804512.
(128) Hu, Y.; Jensen, J. O.; Zhang, W.; Cleemann, L. N.; Xing, W.; Bjerrum, N. J.; Li, Q., Hollow Spheres of Iron Carbide Nanoparticles Encased in Graphitic Layers as Oxygen Reduction Catalysts. *Angew. Chem., Int. Ed.* **2014,** *126*, 3749-3753.
(129) Kumar, K.; Gairola, P.; Lions, M.; Ranjbar-Sahraie, N.; Mermoux, M.; Dubau, L.; Zitolo, A.; Jaouen, F.; Maillard, F., Physical and Chemical Considerations for Improving Catalytic Activity and Stability of Non-Precious-Metal Oxygen Reduction Reaction Catalysts. *ACS Catal.* **2018,** *8*, 11264-11276.
(130) Choi, C. H.; Choi, W. S.; Kasian, O.; Mechler, A. K.; Sougrati, M. T.; Brüller, S.; Strickland, K.; Jia, Q.; Mukerjee, S.; Mayrhofer, K. J.; Jaouen, F., Unraveling the Nature of Sites Active toward Hydrogen Peroxide Reduction in Fe-N-C Catalysts. *Angew. Chem., Int. Ed.* **2017,** *56*, 8809-8812.
(131) Choi, C. H.; Baldizzone, C.; Grote, J. P.; Schuppert, A. K.; Jaouen, F.; Mayrhofer, K. J., Stability of Fe-N-C Catalysts in Acidic Medium Studied by Operando Spectroscopy. *Angew. Chem., Int. Ed.* **2015,** *54*, 12753-12757.
(132) Choi, C. H.; Baldizzone, C.; Polymeros, G.; Pizzutilo, E.; Kasian, O.; Schuppert, A. K.; Ranjbar Sahraie, N.; Sougrati, M.-T.; Mayrhofer, K. J.; Jaouen, F., Minimizing Operando Demetallation of Fe-NC Electrocatalysts in Acidic Medium. *ACS Catal.* **2016,** *6*, 3136-3146.
(133) Ferrandon, M.; Kropf, A. J.; Myers, D. J.; Artyushkova, K.; Kramm, U.; Bogdanoff, P.; Wu, G.; Johnston, C. M.; Zelenay, P., Multitechnique Characterization of a Polyaniline-Iron-Carbon Oxygen Reduction Catalyst. *J. Phys. Chem. C* **2012,** *116*, 16001-16013.
(134) Kramm, U. I.; Herrmann-Geppert, I.; Fiechter, S.; Zehl, G.; Zizak, I.; Dorbandt, I.; Schmeißer, D.; Bogdanoff, P., Effect of Iron-Carbide Formation on the Number of Active Sites in Fe-N-C Catalysts for the Oxygen Reduction Reaction in Acidic Media. *J. Mater. Chem. A* **2014,** *2*, 2663-2670.
(135) Zhang, X.; Truong-Phuoc, L.; Liao, X.; Tuci, G.; Fonda, E.; Papaefthymiou, V.; Zafeiratos, S.; Giambastiani, G.; Pronkin, S.; Pham-Huu, C., An Open Gate for High-Density Metal Ions in N-Doped Carbon Networks: Powering Fe-N-C Catalyst Efficiency in the Oxygen Reduction Reaction. *ACS Catal.* **2021,** *11*, 8915-8928.
(136) Tavakkoli, M.; Kallio, T.; Reynaud, O.; Nasibulin, A. G.; Johans, C.; Sainio, J.; Jiang, H.; Kauppinen, E. I.; Laasonen, K., Single-Shell Carbon-Encapsulated Iron Nanoparticles: Synthesis and High Electrocatalytic Activity for Hydrogen Evolution Reaction. *Angew. Chem., Int. Ed.* **2015,** *54*, 4535-4538.
(137) Chung, D. Y.; Jun, S. W.; Yoon, G.; Kwon, S. G.; Shin, D. Y.; Seo, P.; Yoo, J. M.; Shin, H.; Chung, Y.-H.; Kim, H.; Mun, B. S.; Lee, K.-S.; Lee, N.-S.; Yoo, S. J.; Lim, D.-H.; Kang, K.; Sung, Y.-E.; Hyeon, T., Highly Durable and Active PtFe Nanocatalyst for Electrochemical Oxygen Reduction Reaction. *J.*

Am. Chem. Soc. **2015,** *137*, 15478-15485.
(138) Artyushkova, K.; Serov, A.; Rojas-Carbonell, S.; Atanassov, P., Chemistry of Multitudinous Active Sites for Oxygen Reduction Reaction in Transition Metal-Nitrogen-Carbon Electrocatalysts. *J. Phys. Chem. C* **2015,** *119*, 25917-25928.
(139) Matanovic, I.; Artyushkova, K.; Atanassov, P., Understanding PGM-Free Catalysts by Linking Density Functional Theory Calculations and Structural Analysis: Perspectives and Challenges. *Curr. Opin. Electrochem.* **2018,** *9*, 137-144.
(140) Matanovic, I.; Artyushkova, K.; Strand, M. B.; Dzara, M. J.; Pylypenko, S.; Atanassov, P., Core Level Shifts of Hydrogenated Pyridinic and Pyrrolic Nitrogen in the Nitrogen-Containing Graphene-Based Electrocatalysts: In-Plane Vs Edge Defects. *J. Phys. Chem. C* **2016,** *120*, 29225-29232.
(141) Mamtani, K.; Jain, D.; Zemlyanov, D.; Celik, G.; Luthman, J.; Renkes, G.; Co, A. C.; Ozkan, U. S., Probing the Oxygen Reduction Reaction Active Sites over Nitrogen-Doped Carbon Nanostructures (CN_x) in Acidic Media Using Phosphate Anion. *ACS Catal.* **2016,** *6*, 7249-7259.
(142) Chen, Y.; Matanovic, I.; Weiler, E.; Atanassov, P.; Artyushkova, K., Mechanism of Oxygen Reduction Reaction on Transition Metal-Nitrogen-Carbon Catalysts: Establishing the Role of Nitrogen-Containing Active Sites. *ACS Appl. Energy Mater.* **2018,** *1*, 5948-5953.
(143) Kabir, S.; Artyushkova, K.; Serov, A.; Atanassov, P., Role of Nitrogen Moieties in N-Doped 3d-Graphene Nanosheets for Oxygen Electroreduction in Acidic and Alkaline Media. *ACS Appl. Mater. Interfaces* **2018,** *10*, 11623-11632.
(144) Guo, D.; Shibuya, R.; Akiba, C.; Saji, S.; Kondo, T.; Nakamura, J., Active Sites of Nitrogen-Doped Carbon Materials for Oxygen Reduction Reaction Clarified Using Model Catalysts. *Science* **2016,** *351*, 361-365.
(145) Kondo, T.; Casolo, S.; Suzuki, T.; Shikano, T.; Sakurai, M.; Harada, Y.; Saito, M.; Oshima, M.; Trioni, M. I.; Tantardini, G. F.; Nakamura, J., Atomic-Scale Characterization of Nitrogen-Doped Graphite: Effects of Dopant Nitrogen on the Local Electronic Structure of the Surrounding Carbon Atoms. *Phys. Rev. B* **2012,** *86*, 035436-035441.
(146) Wan, K.; Yu, Z.-p.; Li, X.-h.; Liu, M.-y.; Yang, G.; Piao, J.-h.; Liang, Z.-x., pH Effect on Electrochemistry of Nitrogen-Doped Carbon Catalyst for Oxygen Reduction Reaction. *ACS Catal.* **2015,** *5*, 4325-4332.
(147) Li, X.; Liu, G.; Popov, B. N., Activity and Stability of Non-Precious Metal Catalysts for Oxygen Reduction in Acid and Alkaline Electrolytes. *J. Power Sources* **2010,** *195*, 6373-6378.
(148) Ochal, P.; de la Fuente, J. L. G.; Tsypkin, M.; Seland, F.; Sunde, S.; Muthuswamy, N.; Rønning, M.; Chen, D.; Garcia, S.; Alayoglu, S.; Bryan, E., CO Stripping as an Electrochemical Tool for Characterization of Ru@Pt Core-Shell Catalysts. *J. Electroanal. Chem.* **2011,** *655*, 140-146.
(149) Vidakovic, T.; Christov, M.; Sundmacher, K., The Use of CO Stripping for in Situ Fuel Cell Catalyst Characterization. *Electrochim. Acta* **2007,** *52*, 5606-5613.
(150) Birry, L.; Zagal, J. H.; Dodelet, J.-P., Does CO Poison Fe-Based Catalysts for ORR? *Electrochem. Commun.* **2010,** *12*, 628-631.
(151) Zhang, Q.; Mamtani, K.; Jain, D.; Ozkan, U.; Asthagiri, A., CO Poisoning Effects on FeNC and CN_x ORR Catalysts: A Combined Experimental-Computational Study. *J. Phys. Chem. C* **2016,** *120*, 15173-15184.
(152) Chung, M. W.; Chon, G.; Kim, H.; Jaouen, F.; Choi, C. H., Electrochemical Evidence for Two Sub-Families of FeN_xC_y Moieties with Concentration-Dependent Cyanide Poisoning. *ChemElectroChem* **2018,** *5*, 1880-1885.

(153) Thorum, M. S.; Hankett, J. M.; Gewirth, A. A., Poisoning the Oxygen Reduction Reaction on Carbon-Supported Fe and Cu Electrocatalysts: Evidence for Metal-Centered Activity. *J. Phys. Chem. Lett.* **2011,** *2*, 295-298.
(154) Bae, G.; Kim, H.; Choi, H.; Jeong, P.; Kim, D. H.; Kwon, H. C.; Lee, K.-S.; Choi, M.; Oh, H.-S.; Jaouen, F.; Choi, C. H., Quantification of Active Site Density and Turnover Frequency: From Single-Atom Metal to Nanoparticle Electrocatalysts. *JACS Au* **2021,** *1*, 586-597.
(155) Singh, D.; Mamtani, K.; Bruening, C. R.; Miller, J. T.; Ozkan, U. S., Use of H_2S to Probe the Active Sites in FeNC Catalysts for the Oxygen Reduction Reaction (ORR) in Acidic Media. *ACS Catal.* **2014,** *4*, 3454-3462.
(156) Wang, Q.; Zhou, Z.-Y.; Lai, Y.-J.; You, Y.; Liu, J.-G.; Wu, X.-L.; Terefe, E.; Chen, C.; Song, L.; Rauf, M.; Tian, N.; Sun, S.-G., Phenylenediamine-Based FeN_x/C Catalyst with High Activity for Oxygen Reduction in Acid Medium and Its Active-Site Probing. *J. Am. Chem. Soc.* **2014,** *136*, 10882-10885.
(157) Sahraie, N. R.; Kramm, U. I.; Steinberg, J.; Zhang, Y.; Thomas, A.; Reier, T.; Paraknowitsch, J.-P.; Strasser, P., Quantifying the Density and Utilization of Active Sites in Non-Precious Metal Oxygen Electroreduction Catalysts. *Nat. Commun.* **2015,** *6*, 1-9.
(158) Malko, D.; Kucernak, A.; Lopes, T., In Situ Electrochemical Quantification of Active Sites in Fe–N/C Non-Precious Metal Catalysts. *Nat. Commun.* **2016,** *7*, 1-7.
(159) Wan, X.; Liu, X.; Li, Y.; Yu, R.; Zheng, L.; Yan, W.; Wang, H.; Xu, M.; Shui, J., Fe-N-C Electrocatalyst with Dense Active Sites and Efficient Mass Transport for High-Performance Proton Exchange Membrane Fuel Cells. *Nat. Catal.* **2019,** *2*, 259-268.
(160) Kumar, K.; Asset, T.; Li, X.; Liu, Y.; Yan, X.; Chen, Y.; Mermoux, M.; Pan, X.; Atanassov, P.; Maillard, F.; Dubau, L., Fe-N-C Electrocatalysts' Durability: Effects of Single Atoms' Mobility and Clustering. *ACS Catal.* **2020,** *11*, 484-494.
(161) Jean, Y., *Molecular Orbitals of Transition Metal Complexes*. OUP Oxford: 2005, 24-29.
(162) Zagal, J. H.; Bedioui, F.; Dodelet, J.-P., *N_4-Macrocyclic Metal Complexes*. Springer Science & Business Media: 2007, 46-48.
(163) Liu, K.; Lei, Y.; Wang, G., Correlation between Oxygen Adsorption Energy and Electronic Structure of Transition Metal Macrocyclic Complexes. *J. Chem. Phys.* **2013,** *139*, 204306-204314.
(164) Seo, M. H.; Higgins, D.; Jiang, G.; Choi, S. M.; Han, B.; Chen, Z., Theoretical Insight into Highly Durable Iron Phthalocyanine Derived Non-Precious Catalysts for Oxygen Reduction Reactions. *J. Mater. Chem. A* **2014,** *2*, 19707-19716.
(165) Ramaswamy, N.; Tylus, U.; Jia, Q.; Mukerjee, S., Activity Descriptor Identification for Oxygen Reduction on Nonprecious Electrocatalysts: Linking Surface Science to Coordination Chemistry. *J. Am. Chem. Soc.* **2013,** *135*, 15443-15449.
(166) Bakandritsos, A.; Kadam, R. G.; Kumar, P.; Zoppellaro, G.; Medved', M.; Tuček, J.; Montini, T.; Tomanec, O.; Andrýsková, P.; Drahoš, B.; Varma, R. S.; Otyepka, M.; Gawande, M. B.; Fornasiero, P.; Zbořil, R., Mixed-Valence Single-Atom Catalyst Derived from Functionalized Graphene. *Adv. Mater.* **2019,** *31*, 1900323-1900331.
(167) Men, B.; Sun, Y.; Liu, J.; Tang, Y.; Chen, Y.; Wan, P.; Pan, J., Synergistically Enhanced Electrocatalytic Activity of Sandwich-Like N-Doped Graphene/Carbon Nanosheets Decorated by Fe and S for Oxygen Reduction Reaction. *ACS Appl. Mater. Interfaces* **2016,** *8*, 19533-19541.
(168) Kwak, D.-H.; Han, S.-B.; Lee, Y.-W.; Park, H.-S.; Choi, I.-A.; Ma, K.-B.; Kim, M.-C.; Kim, S.-J.; Kim, D.-H.; Sohn, J.-I.; Park, K.-W., Fe/N/S-Doped Mesoporous Carbon Nanostructures as Electrocatalysts for Oxygen Reduction Reaction in Acid Medium. *Appl. Catal. B: Environ.* **2017,** *203*,

889-898.
(169) Jin, H.; Zhou, H.; He, D.; Wang, Z.; Wu, Q.; Liang, Q.; Liu, S.; Mu, S., MOF-Derived 3D Fe-NS Co-Doped Carbon Matrix/Nanotube Nanocomposites with Advanced Oxygen Reduction Activity and Stability in Both Acidic and Alkaline Media. *Appl. Catal. B: Environ.* **2019,** *250*, 143-149.
(170) Kone, I.; Xie, A.; Tang, Y.; Chen, Y.; Liu, J.; Chen, Y.; Sun, Y.; Yang, X.; Wan, P., Hierarchical Porous Carbon Doped with Iron/Nitrogen/Sulfur for Efficient Oxygen Reduction Reaction. *ACS Appl. Mater. Interfaces* **2017,** *9*, 20963-20973.
(171) Sasan, K.; Kong, A.; Wang, Y.; Chengyu, M.; Zhai, Q.; Feng, P., From Hemoglobin to Porous N-S-Fe-Doped Carbon for Efficient Oxygen Electroreduction. *J. Phys. Chem. C* **2015,** *119*, 13545-13550.
(172) Wu, Y.-J.; Wang, Y.-C.; Wang, R.-X.; Zhang, P.-F.; Yang, X.-D.; Yang, H.-J.; Li, J.-T.; Zhou, Y.; Zhou, Z.-Y.; Sun, S.-G., Three-Dimensional Networks of S-Doped Fe/N/C with Hierarchical Porosity for Efficient Oxygen Reduction in Polymer Electrolyte Membrane Fuel Cells. *ACS Appl. Mater. Interfaces* **2018,** *10*, 14602-14613.
(173) Hu, K.; Tao, L.; Liu, D.; Huo, J.; Wang, S., Sulfur-Doped Fe/N/C Nanosheets as Highly Efficient Electrocatalysts for Oxygen Reduction Reaction. *ACS Appl. Mater. Interfaces* **2016,** *8*, 19379-19385.
(174) Zhang, J.; Zhao, Y.; Chen, C.; Huang, Y.-C.; Dong, C.-L.; Chen, C.-J.; Liu, R.-S.; Wang, C.; Yan, K.; Li, Y.; Wang, G., Tuning the Coordination Environment in Single-Atom Catalysts to Achieve Highly Efficient Oxygen Reduction Reactions. *J. Am. Chem. Soc.* **2019,** *141*, 20118-20126.
(175) Li, Q.; Chen, W.; Xiao, H.; Gong, Y.; Li, Z.; Zheng, L.; Zheng, X.; Yan, W.; Cheong, W. C.; Shen, R.; Fu, N.; Gu, L.; Zhuang, Z.; Chen, C.; Wang, D.; Peng, Q.; Li, J.; Li, Y., Fe Isolated Single Atoms on S, N Codoped Carbon by Copolymer Pyrolysis Strategy for Highly Efficient Oxygen Reduction Reaction. *Adv. Mater.* **2018,** *30*, 1800588-1800593.
(176) Mun, Y.; Lee, S.; Kim, K.; Kim, S.; Lee, S.; Han, J. W.; Lee, J., Versatile Strategy for Tuning ORR Activity of a Single Fe-N_4 Site by Controlling Electron-Withdrawing/Donating Properties of a Carbon Plane. *J. Am. Chem. Soc.* **2019,** *141*, 6254-6262.
(177) Ni, B.; Chen, R.; Wu, L.; Xu, X.; Shi, C.; Sun, P.; Chen, T., Optimized Enhancement Effect of Sulfur in Fe-N-S Codoped Carbon Nanosheets for Efficient Oxygen Reduction Reaction. *ACS Appl. Mater. Interfaces* **2020,** *12*, 23995-24006.
(178) Shen, H.; Gracia-Espino, E.; Ma, J.; Zang, K.; Luo, J.; Wang, L.; Gao, S.; Mamat, X.; Hu, G.; Wagberg, T.; Guo, S., Synergistic Effects between Atomically Dispersed Fe-N-C and C-S-C for the Oxygen Reduction Reaction in Acidic Media. *Angew. Chem., Int. Ed.* **2017,** *129*, 13988-13992.
(179) Fajrial, A. K.; Saputro, A. G.; Agusta, M. K.; Rusydi, F.; Dipojono, H. K., First Principles Study of Oxygen Molecule Interaction with the Graphitic Active Sites of a Boron-Doped Pyrolyzed Fe-N-C Catalyst. *Phys. Chem. Chem. Phys.* **2017,** *19*, 23497-23504.
(180) Yuan, K.; Sfaelou, S.; Qiu, M.; Lützenkirchen-Hecht, D.; Zhuang, X.; Chen, Y.; Yuan, C.; Feng, X.; Scherf, U., Synergetic Contribution of Boron and Fe-N_x Species in Porous Carbons toward Efficient Electrocatalysts for Oxygen Reduction Reaction. *ACS Energy Lett.* **2017,** *3*, 252-260.
(181) Yuan, K.; Lutzenkirchen-Hecht, D.; Li, L.; Shuai, L.; Li, Y.; Cao, R.; Qiu, M.; Zhuang, X.; Leung, M. K.; Chen, Y.; Scherf, U., Boosting Oxygen Reduction of Single Iron Active Sites Via Geometric and Electronic Engineering: Nitrogen and Phosphorus Dual Coordination. *J. Am. Chem. Soc.* **2020,** *142*, 2404-2412.
(182) Yin, H.; Yuan, P.; Lu, B.-A.; Xia, H.; Guo, K.; Yang, G.; Qu, G.; Xue, D.; Hu, Y.; Cheng, J.; Mu, S.; Zhang, J., Phosphorus-Driven Electron Delocalization on Edge-Type FeN_4 Active Sites for Oxygen Reduction in Acid Medium. *ACS Catal.* **2021,** *11*, 12754-12762.

(183) Chen, Y.; Ji, S.; Zhao, S.; Chen, W.; Dong, J.; Cheong, W.-C.; Shen, R.; Wen, X.; Zheng, L.; Rykov, A. I.; Cai, S.; Tang, H.; Zhuang, Z.; Chen, C.; Peng, Q.; Wang, D.; Li, Y., Enhanced Oxygen Reduction with Single-Atomic-Site Iron Catalysts for a Zinc-Air Battery and Hydrogen-Air Fuel Cell. *Nat. Commun.* **2018,** *9*, 1-12.
(184) Ni, W.; Gao, Y.; Zhang, Y.; Younus, H. A.; Guo, X.; Ma, C.; Zhang, Y.; Duan, J.; Zhang, J.; Zhang, S., O-Doping Boosts the Electrochemical Oxygen Reduction Activity of a Single Fe Site in Hydrophilic Carbon with Deep Mesopores. *ACS Appl. Mater. Interfaces* **2019,** *11*, 45825-45831.
(185) Chen, C.; Kang, Y.; Huo, Z.; Zhu, Z.; Huang, W.; Xin, H. L.; Snyder, J. D.; Li, D.; Herron, J. A.; Mavrikakis, M.; Chi, M.; More, K. L.; Li, Y.; Markovic, N. M.; Somorjai, G. A.; Yang, P.; Stamenković, V. R., Highly Crystalline Multimetallic Nanoframes with Three-Dimensional Electrocatalytic Surfaces. *Science* **2014,** *343*, 1339-1343.
(186) Dubau, L.; Lopez-Haro, M.; Castanheira, L.; Durst, J.; Chatenet, M.; Bayle-Guillemaud, P.; Guétaz, L.; Caqué, N.; Rossinot, E.; Maillard, F., Probing the Structure, the Composition and the ORR Activity of Pt_3Co/C Nanocrystallites During a 3422 h PEMFC Ageing Test. *Appl. Catal. B: Environ.* **2013,** *142*, 801-808.
(187) Asset, T.; Gommes, C. J.; Drnec, J.; Bordet, P.; Chattot, R.; Martens, I.; Nelayah, J.; Job, N.; Maillard, F.; Dubau, L., Disentangling the Degradation Pathways of Highly Defective PtNi/C Nanostructures-an Operando Wide and Small Angle X-Ray Scattering Study. *ACS Catal.* **2018,** *9*, 160-167.
(188) Holdcroft, S., Fuel Cell Catalyst Layers: A Polymer Science Perspective. *Chem. Mater.* **2014,** *26*, 381-393.
öö
(189) Ott, S.; Orfanidi, A.; Schmies, H.; Anke, B.; Nong, H. N.; Hübner, J.; Gernert, U.; Gliech, M.; Lerch, M.; Strasser, P., Ionomer Distribution Control in Porous Carbon-Supported Catalyst Layers for High-Power and Low Pt-Loaded Proton Exchange Membrane Fuel Cells. *Nat. Mater.* **2020,** *19*, 77-85.
(190) Zhao, Z.; Hossain, M. D.; Xu, C.; Lu, Z.; Liu, Y.-S.; Hsieh, S.-H.; Lee, I.; Gao, W.; Yang, J.; Merinov, B. V.; Xue, W.; Liu, Z.; Zhou, J.; Luo, Z.; Pan, X.; Zaera, F.; Guo, J.; Duan, X.; Goddard III, W. A.; Huang, Y., Tailoring a Three-Phase Microenvironment for High-Performance Oxygen Reduction Reaction in Proton Exchange Membrane Fuel Cells. *Matter* **2020,** *3*, 1774-1790.
(191) Harada, M.; Kudo, K.; Yamada, N. L., Compositional Segregation in a Cross Section of Wet Nafion Thin Film on a Platinum Surface. *Chem. Lett.* **2019,** *48*, 51-54.
(192) Takeshita, T.; Kamitaka, Y.; Shinozaki, K.; Kodama, K.; Morimoto, Y., Evaluation of Ionomer Coverage on Pt Catalysts in Polymer Electrolyte Membrane Fuel Cells by CO Stripping Voltammetry and Its Effect on Oxygen Reduction Reaction Activity. *J. Electroanal. Chem.* **2020,** *871*, 114250-114256.
(193) Yamada, H.; Kato, H.; Kodama, K., Cell Performance and Durability of Pt/C Cathode Catalyst Covered by Dopamine Derived Carbon Thin Layer for Polymer Electrolyte Fuel Cells. *J. Electrochem. Soc.* **2020,** *167*, 084508.
(194) Padgett, E.; Andrejevic, N.; Liu, Z.; Kongkanand, A.; Gu, W.; Moriyama, K.; Jiang, Y.; Kumaraguru, S.; Moylan, T. E.; Kukreja, R.; Mulller, D. A., Connecting Fuel Cell Catalyst Nanostructure and Accessibility Using Quantitative Cryo-STEM Tomography. *J. Electrochem. Soc.* **2018,** *165*, F173-F180.
(195) Kongkanand, A.; Subramanian, N. P.; Yu, Y.; Liu, Z.; Igarashi, H.; Muller, D. A., Achieving High-Power PEM Fuel Cell Performance with an Ultralow-Pt-Content Core-Shell Catalyst. *ACS Catal.* **2016,** *6*, 1578-1583.

(196) Banham, D.; Kishimoto, T.; Zhou, Y.; Sato, T.; Bai, K.; Ozaki, J.-i.; Imashiro, Y.; Ye, S., Critical Advancements in Achieving High Power and Stable Nonprecious Metal Catalyst-Based MEAs for Real-World Proton Exchange Membrane Fuel Cell Applications. *Sci. Adv.* **2018,** *4*, eaar7180-eaar7186.
(197) Yin, X.; Lin, L.; Chung, H. T.; Babu, S. K.; Martinez, U.; Purdy, G. M.; Zelenay, P., Effects of MEA Fabrication and Ionomer Composition on Fuel Cell Performance of PGM-Free ORR Catalyst. *ECS Trans.* **2017,** *77*, 1273-1281.
(198) Jaouen, F.; Jones, D.; Coutard, N.; Artero, V.; Strasser, P.; Kucernak, A., Toward Platinum Group Metal-Free Catalysts for Hydrogen/Air Proton-Exchange Membrane Fuel Cells. *Johns. Matthey Technol. Rev.* **2018,** *62*, 231-255.
(199) Banham, D.; Choi, J. Y.; Kishimoto, T.; Ye, S., Integrating PGM-Free Catalysts into Catalyst Layers and Proton Exchange Membrane Fuel Cell Devices. *Adv. Mater.* **2019,** *31*, 1804846-1804851.
(200) Liu, J.; Talarposhti, M. R.; Asset, T.; Sabarirajan, D. C.; Parkinson, D. Y.; Atanassov, P.; Zenyuk, I. V., Understanding the Role of Interfaces for Water Management in Platinum Group Metal-Free Electrodes in Polymer Electrolyte Fuel Cells. *ACS Appl. Energy Mater.* **2019,** *2*, 3542-3553.
(201) Jiao, L.; Li, J.; Richard, L. L.; Sun, Q.; Stracensky, T.; Liu, E.; Sougrati, M. T.; Zhao, Z.; Yang, F.; Zhong, S.; Xu, H.; Mukerjee, S.; Huang, Y.; Cullen, D. A.; Park, J.; Ferrandon, M.; Myers, D. J.; Jaouen, F.; Jia, Q., Chemical Vapour Deposition of Fe-N-C Oxygen Reduction Catalysts with Full Utilization of Dense Fe-N_4 Sites. *Nat. Mater.* **2021,** *20*, 1385-1391.
(202) Lee, S. H.; Kim, J.; Chung, D. Y.; Yoo, J. M.; Lee, H. S.; Kim, M. J.; Mun, B. S.; Kwon, S. G.; Sung, Y.-E.; Hyeon, T., Design Principle of Fe-N-C Electrocatalysts: How to Optimize Multimodal Porous Structures? *J. Am. Chem. Soc.* **2019,** *141*, 2035-2045.
(203) Wang, G.; Osmieri, L.; Star, A. G.; Pfeilsticker, J.; Neyerlin, K. C., Elucidating the Role of Ionomer in the Performance of Platinum Group Metal-Free Catalyst Layer Via in Situ Electrochemical Diagnostics. *J. Electrochem. Soc.* **2020,** *167*, 044519-044527.
(204) Uddin, A.; Dunsmore, L.; Zhang, H.; Hu, L.; Wu, G.; Litster, S., High Power Density Platinum Group Metal-Free Cathodes for Polymer Electrolyte Fuel Cells. *ACS Appl. Mater. Interfaces* **2019,** *12*, 2216-2224.
(205) Artyushkova, K.; Workman, M. J.; Matanovic, I.; Dzara, M. J.; Ngo, C.; Pylypenko, S.; Serov, A.; Atanassov, P., Role of Surface Chemistry on Catalyst/Ionomer Interactions for Transition Metal-Nitrogen-Carbon Electrocatalysts. *ACS Appl. Energy Mater.* **2017,** *1*, 68-77.
(206) Wang, Y. C.; Lai, Y. J.; Song, L.; Zhou, Z. Y.; Liu, J. G.; Wang, Q.; Yang, X. D.; Chen, C.; Shi, W.; Zheng, Y. P.; Rauf, M.; Sun, S.-G., S-Doping of an Fe/N/C ORR Catalyst for Polymer Electrolyte Membrane Fuel Cells with High Power Density. *Angew. Chem., Int. Ed.* **2015,** *127*, 10045-10048.
(207) Barkholtz, H. M.; Chong, L.; Kaiser, Z. B.; Xu, T.; Liu, D.-J., Highly Active Non-PGM Catalysts Prepared from Metal Organic Frameworks. *Catalysts* **2015,** *5*, 955-965.
(208) Chung, H. T.; Cullen, D. A.; Higgins, D.; Sneed, B. T.; Holby, E. F.; More, K. L.; Zelenay, P., Direct Atomic-Level Insight into the Active Sites of a High-Performance PGM-Free ORR Catalyst. *Science* **2017,** *357*, 479-484.
(209) Fu, X.; Zamani, P.; Choi, J. Y.; Hassan, F. M.; Jiang, G.; Higgins, D. C.; Zhang, Y.; Hoque, M. A.; Chen, Z., In Situ Polymer Graphenization Ingrained with Nanoporosity in a Nitrogenous Electrocatalyst Boosting the Performance of Polymer-Electrolyte-Membrane Fuel Cells. *Adv. Mater.* **2017,** *29*, 1604456-1604463.
(210) Liu, Q.; Liu, X.; Zheng, L.; Shui, J., The Solid-Phase Synthesis of an Fe-N-C Electrocatalyst for High-Power Proton-Exchange Membrane Fuel Cells. *Angew. Chem., Int. Ed.* **2018,** *130*, 1218-1222.

(211) Li, J.; Zhang, H.; Samarakoon, W.; Shan, W.; Cullen, D. A.; Karakalos, S.; Chen, M.; Gu, D.; More, K. L.; Wang, G.; Feng, Z.; Wang, Z.; Wu, G., Thermally Driven Structure and Performance Evolution of Atomically Dispersed FeN_4 Sites for Oxygen Reduction. *Angew. Chem., Int. Ed.* **2019,** *131*, 19147-19156.
(212) Zhang, H.; Chung, H. T.; Cullen, D. A.; Wagner, S.; Kramm, U. I.; More, K. L.; Zelenay, P.; Wu, G., High-Performance Fuel Cell Cathodes Exclusively Containing Atomically Dispersed Iron Active Sites. *Energy Environ. Sci.* **2019,** *12*, 2548-2558.
(213) Liu, S.; Wang, M.; Yang, X.; Shi, Q.; Qiao, Z.; Lucero, M.; Ma, Q.; More, K. L.; Cullen, D. A.; Feng, Z.; Wu, G., Chemical Vapor Deposition for Atomically Dispersed and Nitrogen Coordinated Single Metal Site Catalysts. *Angew. Chem., Int. Ed.* **2020,** *59*, 21698-21705.
(214) Zhao, X.; Yang, X.; Wang, M.; Hwang, S.; Karakalos, S.; Chen, M.; Qiao, Z.; Wang, L.; Liu, B.; Ma, Q.; Cullen, D. A.; Su, D.; Yang, H.; Zhang, H.-Y.; Feng, Z.; Wu, G., Single-Iron Site Catalysts with Self-Assembled Dual-Size Architecture and Hierarchical Porosity for Proton-Exchange Membrane Fuel Cells. *Appl. Catal. B: Environ.* **2020,** *279*, 119400.
(215) Wang, Q.; Yang, Y.; Sun, F.; Chen, G.; Wang, J.; Peng, L.; Chen, W. T.; Shang, L.; Zhao, J.; Sun-Waterhouse, D.; Zhang, T.; Waterhouse, G. I., Molten NaCl-Assisted Synthesis of Porous Fe-N-C Electrocatalysts with a High Density of Catalytically Accessible FeN_4 Active Sites and Outstanding Oxygen Reduction Reaction Performance. *Adv. Energy Mater.* **2021,** *11*, 2100219-2100227.
(216) Mehmood, A.; Gong, M.; Jaouen, F.; Roy, A.; Zitolo, A.; Khan, A.; Sougrati, M. T.; Primbs, M.; Bonastre, A. M.; Fongalland, D.; Drazic, G.; Strasser, P.; Kucernak, A., High Loading of Single Atomic Iron Sites in Fe–NC Oxygen Reduction Catalysts for Proton Exchange Membrane Fuel Cells. *Nat. Catal.* **2022,** *5*, 311–323.
(217) Han, B.; Carlton, C. E.; Kongkanand, A.; Kukreja, R. S.; Theobald, B. R.; Gan, L.; O'Malley, R.; Strasser, P.; Wagner, F. T.; Shao-Horn, Y., Record Activity and Stability of Dealloyed Bimetallic Catalysts for Proton Exchange Membrane Fuel Cells. *Energy Environ. Sci.* **2015,** *8*, 258-266.
(218) Kim, H. Y.; Cho, S.; Sa, Y. J.; Hwang, S. M.; Park, G. G.; Shin, T. J.; Jeong, H. Y.; Yim, S. D.; Joo, S. H., Self-Supported Mesostructured Pt-Based Bimetallic Nanospheres Containing an Intermetallic Phase as Ultrastable Oxygen Reduction Electrocatalysts. *Small* **2016,** *12*, 5347-5353.
(219) Dionigi, F.; Weber, C. C.; Primbs, M.; Gocyla, M.; Bonastre, A. M.; Spori, C.; Schmies, H.; Hornberger, E.; Kuhl, S.; Drnec, J.; Heggen, M.; Sharman, J.; Edward Dunin-Borkowski, R.; Strasser, P., Controlling near-Surface Ni Composition in Octahedral PtNi (Mo) Nanoparticles by Mo Doping for a Highly Active Oxygen Reduction Reaction Catalyst. *Nano lett.* **2019,** *19*, 6876-6885.
(220) Spendelow, J. S., Advanced Electro-Catalysts through Crystallographic Enhancement. *DOE Hydrogen and Fuel Cells Program2020 Annual Merit Review (Energy USDo, 2020)* **2019**.
(221) Li, J.; Sharma, S.; Liu, X.; Pan, Y.-T.; Spendelow, J. S.; Chi, M.; Jia, Y.; Zhang, P.; Cullen, D. A.; Xi, Z.; Lin, H.; Yin, Z.; Shen, B.; Muzzio, M.; Yu, C.; Kim, Y. S.; Peterson, D. A.; More, K. L.; Zhu, H.; Sun, S., Hard-Magnet L10-CoPt Nanoparticles Advance Fuel Cell Catalysis. *Joule* **2019,** *3*, 124-135.
(222) Duclos, L.; Chattot, R.; Dubau, L.; Thivel, P.-X.; Mandil, G.; Laforest, V.; Bolloli, M.; Vincent, R.; Svecova, L., Closing the Loop: Life Cycle Assessment and Optimization of a PEMFC Platinum-Based Catalyst Recycling Process. *Green Chem.* **2020,** *22*, 1919-1933.
(223) Zhao, L.; Zhang, Y.; Huang, L.-B.; Liu, X.-Z.; Zhang, Q.-H.; He, C.; Wu, Z.-Y.; Zhang, L.-J.; Wu, J.; Yang, W.; Gu, L.; Hu, J.-S.; Wan, L.-J., Cascade Anchoring Strategy for General Mass Production of High-Loading Single-Atomic Metal-Nitrogen Catalysts. *Nat. Commun.* **2019,** *10*, 1-11.
(224) Li, J.-C.; Maurya, S.; Kim, Y. S.; Li, T.; Wang, L.; Shi, Q.; Liu, D.; Feng, S.; Lin, Y.; Shao, M., Stabilizing Single-Atom Iron Electrocatalysts for Oxygen Reduction Via Ceria Confining and Trapping.

ACS Catal. **2020,** *10*, 2452-2458.
(225) Zhang, X.; Truong-Phuoc, L.; Liao, X.; Papaefthimiou, V.; Pugliesi, M.; Tuci, G.; Giambastiani, G.; Pronkin, S.; Pham-Huu, C., Inducing Atomically Dispersed Cl-FeN_4 Sites for ORRs in the SiO_2-Mediated Synthesis of Highly Mesoporous N-Enriched C-Networks. *J. Mater. Chem. A* **2022,** *10*, 6153-6164.
(226) Zheng, Y.; Huang, G.; Wang, L.; Varcoe, J. R.; Kohl, P. A.; Mustain, W., Effect of Reacting Gas Flowrates and Hydration on the Carbonation of Anion Exchange Membrane Fuel Cells in the Presence of CO_2. *J. Power Sources* **2020,** *467*, 228350-228357.
(227) Shiau, H.-S.; Zenyuk, I. V.; Weber, A. Z., Elucidating Performance Limitations in Alkaline-Exchange-Membrane Fuel Cells. *J. Electrochem. Soc.* **2017,** *164*, E3583-E3591.
(228) Zheng, Y.; Omasta, T. J.; Peng, X.; Wang, L.; Varcoe, J. R.; Pivovar, B. S.; Mustain, W. E., Quantifying and Elucidating the Effect of CO_2 on the Thermodynamics, Kinetics and Charge Transport of Aemfcs. *Energy Environ. Sci.* **2019,** *12*, 2806-2819.
(229) Kim, S.; Her, M.; Kim, Y.; Ahn, C.-Y.; Park, S.; Cho, Y.-H.; Sung, Y.-E., The Impact of the Catalyst Layer Structure on the Performance of Anion Exchange Membrane Fuel Cell. *Electrochim. Acta* **2021,** *400*, 139439.
(230) Otsuji, K.; Shirase, Y.; Asakawa, T.; Yokota, N.; Nagase, K.; Xu, W.; Song, P.; Wang, S.; Tryk, D. A.; Kakinuma, K.; Inukai, J.; Miyatake, K.; Uchida, M., Effect of Water Management in Membrane and Cathode Catalyst Layers on Suppressing the Performance Hysteresis Phenomenon in Anion-Exchange Membrane Fuel Cells. *J. Power Sources* **2022,** *522*, 230997.
(231) Otsuji, K.; Yokota, N.; Tryk, D. A.; Kakinuma, K.; Miyatake, K.; Uchida, M., Performance Hysteresis Phenomena of Anion Exchange Membrane Fuel Cells Using an Fe-N-C Cathode Catalyst and an in-House-Developed Polymer Electrolyte. *J. Power Sources* **2021,** *487*, 229407.
(232) Zhang, J.; Zhu, W.; Huang, T.; Zheng, C.; Pei, Y.; Shen, G.; Nie, Z.; Xiao, D.; Yin, Y.; Guiver, M. D., Recent Insights on Catalyst Layers for Anion Exchange Membrane Fuel Cells. *Adv. Sci.* **2021,** *8*, 2100284-2100309.
(233) Adabi, H.; Santori, P. G.; Shakouri, A.; Peng, X.; Yassin, K.; Rasin, I. G.; Brandon, S.; Dekel, D. R.; Hassan, N. U.; Sougrati, M.-T.; Zitolo, A.; Varcoe, J. R.; Regalbuto, J. R.; Jaouen, F.; Mustain, W. E., Understanding How Single-Atom Site Density Drives the Performance and Durability of PGM-Free Fe-N-C Cathodes in Anion Exchange Membrane Fuel Cells. *Mater. Today Adv.* **2021,** *12*, 100179.
(234) Lilloja, J.; Kibena-Poldsepp, E.; Sarapuu, A.; Douglin, J. C.; Kaarik, M.; Kozlova, J.; Paiste, P.; Kikas, A.; Aruvali, J.; Leis, J.; Sammelselg, V.; Dekel, D. R.; Tammeveski, K., Transition-Metal-and Nitrogen-Doped Carbide-Derived Carbon/Carbon Nanotube Composites as Cathode Catalysts for Anion-Exchange Membrane Fuel Cells. *ACS Catal.* **2021,** *11*, 1920-1931.
(235) Ul Hassan, N.; Mandal, M.; Huang, G.; Firouzjaie, H. A.; Kohl, P. A.; Mustain, W. E., Achieving High-Performance and 2000 h Stability in Anion Exchange Membrane Fuel Cells by Manipulating Ionomer Properties and Electrode Optimization. *Adv. Energy Mater.* **2020,** *10*, 2001986-2001993.
(236) Santori, P. G. Investigation of Electrocatalysts for Anion-Exchange Membrane Fuel Cells. Université Montpellier, 2019.
(237) Adabi, H.; Shakouri, A.; Ul Hassan, N.; Varcoe, J. R.; Zulevi, B.; Serov, A.; Regalbuto, J. R.; Mustain, W. E., High-Performing Commercial Fe–N–C Cathode Electrocatalyst for Anion-Exchange Membrane Fuel Cells. *Nat. Energy* **2021,** *6*, 834-843.
(238) White, R. T.; Eberhardt, S. H.; Singh, Y.; Haddow, T.; Dutta, M.; Orfino, F. P.; Kjeang, E., Four-Dimensional Joint Visualization of Electrode Degradation and Liquid Water Distribution inside

Operating Polymer Electrolyte Fuel Cells. *Sci. Rep.* **2019,** *9*, 1-12.
(239) Tang, H.; Qi, Z.; Ramani, M.; Elter, J. F., PEM Fuel Cell Cathode Carbon Corrosion Due to the Formation of Air/Fuel Boundary at the Anode. *J. Power Sources* **2006,** *158*, 1306-1312.
(240) Chen, J.; Hu, J.; Waldecker, J. R., A Comprehensive Model for Carbon Corrosion During Fuel Cell Start-Up. *J. Electrochem. Soc.* **2015,** *162*, F878-F889.
(241) Reiser, C. A.; Bregoli, L.; Patterson, T. W.; Jung, S. Y.; Yang, J. D.; Perry, M. L.; Jarvi, T. D., A Reverse-Current Decay Mechanism for Fuel Cells. *Electrochem. Solid-State Lett.* **2005,** *8*, A273-A276.
(242) Wang, W.; Jia, Q.; Mukerjee, S.; Chen, S., Recent Insights into the Oxygen-Reduction Electrocatalysis of Fe/N/C Materials. *ACS Catal.* **2019,** *9*, 10126-10141.
(243) Maillard, F.; O. Silva, W.; Castanheira, L.; Dubau, L.; Lima, F. H., Carbon Corrosion in Proton-Exchange Membrane Fuel Cells: Spectrometric Evidence for Pt-Catalysed Decarboxylation at Anode-Relevant Potentials. *ChemPhysChem* **2019,** *20*, 3106-3111.
(244) Zhao, Z.; Castanheira, L.; Dubau, L.; Berthomé, G.; Crisci, A.; Maillard, F., Carbon Corrosion and Platinum Nanoparticles Ripening under Open Circuit Potential Conditions. *J. Power Sources* **2013,** *230*, 236-243.
(245) Asset, T.; Job, N.; Busby, Y.; Crisci, A.; Martin, V.; Stergiopoulos, V.; Bonnaud, C.; Serov, A.; Atanassov, P.; Chattot, R.; Dubau, L.; Maillard, F., Porous Hollow PtNi/C Electrocatalysts: Carbon Support Considerations to Meet Performance and Stability Requirements. *ACS Catal.* **2018,** *8*, 893-903.
(246) Cremers, C.; Jurzinsky, T.; Meier, J.; Schade, A.; Branghofer, M.; Pinkwart, K.; Tübke, J., DEMS and Online Mass Spectrometry Studies of the Carbon Support Corrosion under Various Polymer Electrolyte Membrane Fuel Cell Operating Conditions. *J. Electrochem. Soc.* **2018,** *165*, F3307-F3315.
(247) Asset, T.; Chattot, R.; Maillard, F.; Dubau, L.; Ahmad, Y.; Batisse, N.; Dubois, M.; Guérin, K.; Labbé, F.; Metkemeijer, R.; Berthon-Fabry, S.; Chatenet, M., Activity and Durability of Platinum-Based Electrocatalysts Supported on Bare or Fluorinated Nanostructured Carbon Substrates. *J. Electrochem. Soc.* **2018,** *165*, F3346-F3358.
(248) Ramaswamy, N.; Kumaraguru, S.; Gu, W.; Kukreja, R. S.; Yu, K.; Groom, D.; Ferreira, P., High-Current Density Durability of Pt/C and PtCo/C Catalysts at Similar Particle Sizes in PEMFCs. *J. Electrochem. Soc.* **2021,** *168*, 024519-024529.
(249) Macauley, N.; Papadias, D. D.; Fairweather, J.; Spernjak, D.; Langlois, D.; Ahluwalia, R.; More, K. L.; Mukundan, R.; Borup, R. L., Carbon Corrosion in PEM Fuel Cells and the Development of Accelerated Stress Tests. *J. Electrochem. Soc.* **2018,** *165*, F3148-F3160.
(250) Dubau, L.; Castanheira, L.; Maillard, F.; Chatenet, M.; Lottin, O.; Maranzana, G.; Dillet, J.; Lamibrac, A.; Perrin, J. C.; Moukheiber, E.; Elkaddouri, A.; De Moor, G.; Bas, C.; Flandin, L.; Caqué, N., A Review of PEM Fuel Cell Durability: Materials Degradation, Local Heterogeneities of Aging and Possible Mitigation Strategies. *Wiley Interdiscip. Rev. Energy Environ.* **2014,** *3*, 540-560.
(251) Sneed, B. T.; Cullen, D. A.; Reeves, K. S.; Dyck, O. E.; Langlois, D. A.; Mukundan, R.; Borup, R. L.; More, K. L., 3D Analysis of Fuel Cell Electrocatalyst Degradation on Alternate Carbon Supports. *ACS Appl. Mater. Interfaces* **2017,** *9*, 29839-29848.
(252) Zhao, Z.; Dubau, L.; Maillard, F., Evidences of the Migration of Pt Crystallites on High Surface Area Carbon Supports in the Presence of Reducing Molecules. *J. Power Sources* **2012,** *217*, 449-458.
(253) Shao-Horn, Y.; Sheng, W.; Chen, S.; Ferreira, P. J.; Holby, E.; Morgan, D., Instability of Supported Platinum Nanoparticles in Low-Temperature Fuel Cells. *Top. Catal.* **2007,** *46*, 285-305.
(254) Ahluwalia, R.; Wang, X.; Peng, J.; Kariuki, N.; Myers, D.; Rasouli, S.; Ferreira, P.; Yang, Z.; Martinez-Bonastre, A.; Fongalland, D.; Sharman, J., Durability of De-Alloyed Platinum-Nickel Cathode

Catalyst in Low Platinum Loading Membrane-Electrode Assemblies Subjected to Accelerated Stress Tests. *J. Electrochem. Soc.* **2018,** *165*, F3316-F3327.
(255) Yasuda, K.; Taniguchi, A.; Akita, T.; Ioroi, T.; Siroma, Z., Platinum Dissolution and Deposition in the Polymer Electrolyte Membrane of a PEM Fuel Cell as Studied by Potential Cycling. *Phys. Chem. Chem. Phys.* **2006,** *8*, 746-752.
(256) Topalov, A. A.; Cherevko, S.; Zeradjanin, A. R.; Meier, J. C.; Katsounaros, I.; Mayrhofer, K. J., Towards a Comprehensive Understanding of Platinum Dissolution in Acidic Media. *Chem. Sci.* **2014,** *5*, 631-638.
(257) Guilminot, E.; Corcella, A.; Chatenet, M.; Maillard, F.; Charlot, F.; Berthomé, G.; Iojoiu, C.; Sanchez, J.-Y.; Rossinot, E.; Claude, E., Membrane and Active Layer Degradation Upon PEMFC Steady-State Operation: I. Platinum Dissolution and Redistribution within the MEA. *J. Electrochem. Soc.* **2007,** *154*, B1106-B1114.
(258) Guilminot, E.; Corcella, A.; Charlot, F.; Maillard, F.; Chatenet, M., Detection of Pt^{z+} Ions and Pt Nanoparticles inside the Membrane of a Used PEMFC. *J. Electrochem. Soc.* **2006,** *154*, B96-B105.
(259) Xie, J.; Wood, D. L.; More, K. L.; Atanassov, P.; Borup, R. L., Microstructural Changes of Membrane Electrode Assemblies During PEFC Durability Testing at High Humidity Conditions. *J. Electrochem. Soc.* **2005,** *152*, A1011-A1020.
(260) Borup, R.; Meyers, J.; Pivovar, B.; Kim, Y. S.; Mukundan, R.; Garland, N.; Myers, D.; Wilson, M.; Garzon, F.; Wood, D.; Zelenay, P.; More, K.; Stroh, K.; Zawodzinski, T.; Boncella, J.; McGrath, J. E.; Inaba, M.; Miyatake, K.; Hori, M.; Ota, K.; Ogumi, Z.; Miyata, S.; Nishikata, A.; Siroma, Z.; Uchimoto, Y.; Yasuda, K.; Kimijima, K.-i.; Iwashita, N., Scientific Aspects of Polymer Electrolyte Fuel Cell Durability and Degradation. *Chem. Rev.* **2007,** *107*, 3904-3951.
(261) Borup, R. L.; Davey, J. R.; Garzon, F. H.; Wood, D. L.; Inbody, M. A., PEM Fuel Cell Electrocatalyst Durability Measurements. *J. Power Sources* **2006,** *163*, 76-81.
(262) Ohyagi, S.; Matsuda, T.; Iseki, Y.; Sasaki, T.; Kaito, C., Effects of Operating Conditions on Durability of Polymer Electrolyte Membrane Fuel Cell Pt Cathode Catalyst Layer. *J. Power Sources* **2011,** *196*, 3743-3749.
(263) Dubau, L.; Maillard, F., Unveiling the Crucial Role of Temperature on the Stability of Oxygen Reduction Reaction Electrocatalysts. *Electrochem. Commun.* **2016,** *63*, 65-69.
(264) Watanabe, M.; Yano, H.; Uchida, H.; Tryk, D., Achievement of Distinctively High Durability at Nanosized Pt Catalysts Supported on Carbon Black for Fuel Cell Cathodes. *J. Electroanal. Chem.* **2018,** *819*, 359-364.
(265) Borup, R. L.; Kusoglu, A.; Neyerlin, K. C.; Mukundan, R.; Ahluwalia, R. K.; Cullen, D. A.; More, K. L.; Weber, A. Z.; Myers, D. J., Recent Developments in Catalyst-Related PEM Fuel Cell Durability. *Curr. Opin. Electrochem.* **2020,** *21*, 192-200.
(266) Sneed, B. T.; Cullen, D. A.; Mukundan, R.; Borup, R. L.; More, K. L., PtCo Cathode Catalyst Morphological and Compositional Changes after PEM Fuel Cell Accelerated Stress Testing. *J. Electrochem. Soc.* **2018,** *165*, F3078-F3084.
(267) Dubau, L.; Nelayah, J.; Asset, T.; Chattot, R. l.; Maillard, F., Implementing Structural Disorder as a Promising Direction for Improving the Stability of PtNi/C Nanoparticles. *ACS Catal.* **2017,** *7*, 3072-3081.
(268) Asset, T.; Chattot, R.; Drnec, J.; Bordet, P.; Job, N.; Maillard, F.; Dubau, L., Elucidating the Mechanisms Driving the Aging of Porous Hollow PtNi/C Nanoparticles by Means of CO_{ads} Stripping. *ACS Appl. Mater. Interfaces* **2017,** *9*, 25298-25307.

(269) Kneer, A.; Jankovic, J.; Susac, D.; Putz, A.; Wagner, N.; Sabharwal, M.; Secanell, M., Correlation of Changes in Electrochemical and Structural Parameters Due to Voltage Cycling Induced Degradation in PEM Fuel Cells. *J. Electrochem. Soc.* **2018,** *165*, F3241-F3250.
(270) Chen, S.; Gasteiger, H. A.; Hayakawa, K.; Tada, T.; Shao-Horn, Y., Platinum-Alloy Cathode Catalyst Degradation in Proton Exchange Membrane Fuel Cells: Nanometer-Scale Compositional and Morphological Changes. *J. Electrochem. Soc.* **2009,** *157*, A82-A97.
(271) Durst, J.; Chatenet, M.; Maillard, F., Impact of Metal Cations on the Electrocatalytic Properties of Pt/C Nanoparticles at Multiple Phase Interfaces. *Phys. Chem. Chem. Phys.* **2012,** *14*, 13000-13009.
(272) Kienitz, B.; Baskaran, H.; Zawodzinski Jr, T., Modeling the Steady-State Effects of Cationic Contamination on Polymer Electrolyte Membranes. *Electrochim. Acta* **2009,** *54*, 1671-1679.
(273) Kienitz, B.; Baskaran, H.; Zawodzinski, T.; Pivovar, B., A Half Cell Model to Study Performance Degradation of a PEMFC Due to Cationic Contamination. *ECS Trans.* **2007,** *11*, 777-788.
(274) Braaten, J.; Kongkanand, A.; Litster, S., Oxygen Transport Effects of Cobalt Cation Contamination of Ionomer Thin Films in Proton Exchange Membrane Fuel Cells. *ECS Trans.* **2017,** *80*, 283-290.
(275) Zhang, G.; Chenitz, R.; Lefèvre, M.; Sun, S.; Dodelet, J.-P., Is Iron Involved in the Lack of Stability of Fe/N/C Electrocatalysts Used to Reduce Oxygen at the Cathode of PEM Fuel Cells? *Nano Energy* **2016,** *29*, 111-125.
(276) Goellner, V.; Baldizzone, C.; Schuppert, A.; Sougrati, M. T.; Mayrhofer, K.; Jaouen, F., Degradation of Fe/N/C Catalysts Upon High Polarization in Acid Medium. *Phys. Chem. Chem. Phys.* **2014,** *16*, 18454-18462.
(277) Martinaiou, I.; Shahraei, A.; Grimm, F.; Zhang, H.; Wittich, C.; Klemenz, S.; Dolique, S. J.; Kleebe, H.-J.; Stark, R. W.; Kramm, U. I., Effect of Metal Species on the Stability of Me-NC Catalysts During Accelerated Stress Tests Mimicking the Start-up and Shut-Down Conditions. *Electrochim. Acta* **2017,** *243*, 183-196.
(278) Choi, C. H.; Lim, H.-K.; Chung, M. W.; Chon, G.; Sahraie, N. R.; Altin, A.; Sougrati, M.-T.; Stievano, L.; Oh, H. S.; Park, E. S.; Luo, F.; Strasser, P.; Drazic, G.; Mayrhofer, K. J.; Kim, H.; Jaouen, F., The Achilles' Heel of Iron-Based Catalysts During Oxygen Reduction in an Acidic Medium. *Energy Environ. Sci.* **2018,** *11*, 3176-3182.